



Published in final edited form as:

Cell. 2018 October 18; 175(3): 665–678.e23. doi:10.1016/j.cell.2018.08.049.

## A Neural Circuit for Gut-Induced Reward

Wenfei Han<sup>1,2,3</sup>, Luis A Tellez<sup>1,2</sup>, Matthew H Perkins<sup>3</sup>, Isaac O. Perez<sup>1,4</sup>, Taoran Qu<sup>1</sup>, Jozelia Ferreira<sup>1,2,5</sup>, Tatiana L Ferreira<sup>1,2,6</sup>, Daniele Quinn<sup>1</sup>, Zhong-Wu Liu<sup>7</sup>, Xiaobing Gao<sup>7</sup>, Melanie M Kaelberer<sup>8</sup>, Diego V Bohórquez<sup>8,9</sup>, Sara J Shammah-Lagnado<sup>10</sup>, Guillaume de Lartigue<sup>1,11</sup>, and Ivan E de Araujo<sup>1,2,3,11,\*</sup>

<sup>1</sup>The John B Pierce Laboratory, New Haven CT, USA

<sup>2</sup>Department of Psychiatry, Yale University School of Medicine, New Haven CT, USA

<sup>3</sup>Fishberg Department of Neuroscience, Icahn School of Medicine at Mount Sinai, New York NY, USA

<sup>4</sup>Section of Neurobiology of Oral Sensations, FES-Iztacala, National Autonomous University of Mexico, Mexico

<sup>5</sup>Department of Anatomy, Biomedical Sciences Institute, University of São Paulo, São Paulo SP, Brazil

<sup>6</sup>Mathematics, Computing and Cognition Center, Federal University of ABC, São Paulo SP, Brazil

<sup>7</sup>Department of Comparative Medicine, Yale University School of Medicine, New Haven CT, USA

<sup>8</sup>Department of Medicine, Duke University, Durham NC, USA

<sup>9</sup>Department of Neurobiology, Duke University, Durham NC, USA

<sup>10</sup>Department of Physiology and Biophysics, Biomedical Sciences Institute, University of São Paulo, Brazil

<sup>11</sup>Department of Physiology, Yale University School of Medicine, New Haven CT, USA

### Abstract

The gut is now recognized as a major regulator of motivational and emotional states. However, the relevant gut-brain neuronal circuitry remains unknown. We show that optical activation of gut-

---

\*Lead Corresponding Author: Ivan E de Araujo, Present address: Fishberg Department of Neuroscience, Icahn School of Medicine at Mount Sinai, New York NY, USA, Ivan.DeAraujo@mssm.edu.

#### Author Contributions

I.E.d.A. conceived study. I.E.d.A., W.H., L.A.T., S.J.S.-L., G.d.L. designed experiments. G.d.L. developed viral approach to nodose. W.H., T.Q., G.d.L. performed gastrointestinal and vagal injections, histology. W.H., L.A.T., M.H.P., T.L.F. J.F. performed stereotaxic surgeries, behavioral, electromyogram and optogenetic experiments, analyzed data. D.Q. performed satiation assays. W.H., S.J.S.-L. performed tracing, histology, imaging. D.V.B., M.M.K. packaged rabies constructs. Z.L., X.G. performed whole-cell patch-clamp experiments, analyzed data. L.A.T. W.H., M.P., I.O.P. performed *in vivo* electrophysiology, analyzed nerve recordings, single-unit data. I.E.d.A. wrote manuscript. All authors interpreted all data, edited manuscript.

**Publisher's Disclaimer:** This is a PDF file of an unedited manuscript that has been accepted for publication. As a service to our customers we are providing this early version of the manuscript. The manuscript will undergo copyediting, typesetting, and review of the resulting proof before it is published in its final citable form. Please note that during the production process errors may be discovered which could affect the content, and all legal disclaimers that apply to the journal pertain.

#### Declaration of Interests

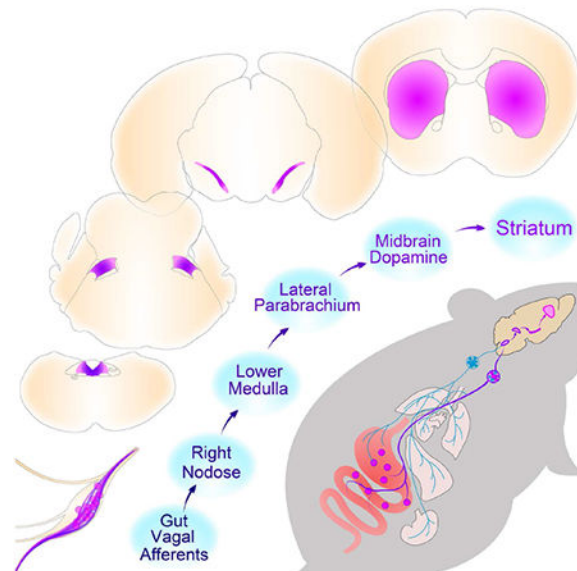
The authors declare no competing interests.

innervating vagal sensory neurons recapitulates the hallmark effects of stimulating brain reward neurons. Specifically, right, but not left, vagal sensory ganglion activation sustained self-stimulation behavior, conditioned both flavor and place preferences, and induced dopamine release from *Substantia nigra*. Cell-specific transneuronal tracing revealed asymmetric ascending pathways of vagal origin throughout the central nervous system. In particular, transneuronal labeling identified the glutamatergic neurons of the dorsolateral parabrachial region as the obligatory relay linking the right vagal sensory ganglion to dopamine cells in *Substantia nigra*. Consistently, optical activation of parabrachio-nigral projections replicated the rewarding effects of right vagus excitation. Our findings establish the vagal gut-to-brain axis as an integral component of the neuronal reward pathway. They also suggest novel vagal stimulation approaches to affective disorders.

## In Brief

A gut to brain neural circuit establishes vagal neurons as an essential component of the reward neuronal circuitry linking sensory neurons in the upper gut to striatal dopamine release.

## Abstract



## Introduction

For centuries, the gastrointestinal branches of the vagus nerve have been recognized as the core of the gut-brain axis (Puizillout, 2005). Conventionally, the function attributed to vagal gut afferents is the transmission of meal-borne signals to the brain, ultimately acting as the chief negative-feedback mechanism for meal size regulation (Schwartz, 2000). In such classical model, gut vagal afferents sensitive to mechanical and chemical signals (Prechtl and Powley, 1990; Williams et al., 2016) act to reduce food reward by engaging their terminal fields in caudal brainstem (Norgren and Smith, 1988; Schwartz, 2000). In contrast,

circulating hormones, rather than vagal transmission, are the factors conventionally believed to convey gut-borne rewarding signals to the brain (Berthoud, 2008; Sclafani, 2013).

More recently, however, a wider range of neuropsychological processes has been attributed to the vagal gut-brain axis. These include anxiety, depression, cognition, and reinforcement (Bohorquez and Liddle, 2015; Clemmensen et al., 2017; de Araujo et al., 2012; Mayer, 2011; Sharon et al., 2016). Still, the neural circuitry allowing gastrointestinal control over motivation and reward remains unmapped. Advances in this field have been greatly limited by the technical difficulties associated with isolating vagal afferents in an organ-specific manner (de Lartigue and Diepenbroek, 2016). To address this question, we made use of virally delivered molecular tools to specify the behavioral functions and central relays of gut-innervating sensory vagal afferents. We focused on challenging the long-held assumption that vagal sensory neurons act to inhibit reward circuits, thereby suppressing motivated behavior (Angyan, 1975).

## Results

### Targeting sensory vagal neurons for gut-brain optogenetics

Our first challenge was to develop an experimental preparation where we could separately manipulate the sensory branch of the vagus nerve. More specifically, we aimed at manipulating the excitability of upper gut-innervating sensory neurons of the vagus. We employed a combinatorial viral approach to achieve our aims. We first transduced the stomach and duodenum of wild-type mice with a retrogradely transported, adeno-associated virus carrying a *Cre*-EBFP construct (AAVrg-pmSyn1-EBFP-*Cre*, Tervo et al., 2016). In this way *Cre* recombinase was retrogradely and bilaterally transported into the sensory ganglia of the vagus nerve (*i.e.* the nodose ganglia, “NG”). Next, we separately transduced the right and left NG with the light-sensitive depolarizing channel *Channelrhodopsin2* by injecting the *Cre*-inducible viral construct AAV-EF1a-DIO-hChR2(H134R)-EYFP (ChR2, Madisen et al., 2012). Since the expression of the light-sensitive channel is *Cre*-dependent, laser pulses would affect only NG neurons expressing *Cre* recombinase – in this case, upper gut-innervating NG neurons retrogradely targeted by upper gut injections of the *Cre*-carrying retrograde virus. The overall viral approach is depicted in Figure 1A.

Upon DIO-ChR2-EYFP injections into the right nodose ganglion (R-NG, Figure 1A and S1A), overlapping expression of AAVrg-pmSyn1-EBFP-*Cre* and DIO-ChR2-EYFP was readily detected in R-NG (Figure, 1B see also S1A). Consistent with a regionally restricted expression of EYFP within R-NG (Figure S1B), confocal microscopy of clarified gut tissue revealed EYFP-positive fibers innervating the upper-gut but no other organs (Figures S1C–E). Nerve recordings obtained upon laser stimulation of the vagal trunk revealed robust, light-locked electrical activity across vagal fibers (Figure 1C). Nerve responses occurred in the absence of detectable changes in gastric motility (Figure S1F).

In the central nervous system, ascending EYFP-positive vagal fibers arising from R-NG were concentrated in ventromedial areas of the nucleus of the solitary tract (NTS; see Figure 1D). In order to achieve stimulation of these gut-innervating R-NG terminals in awake behaving mice, an optic fiber was placed immediately above these NG neuronal terminals in

medial NTS (Figure 1E). Laser pulses delivered through the fiber significantly increased neuronal activity in lower brainstem (Figure S1G).

### **Optical activation of upper gut-innervating vagal sensory neurons induces reward**

We first assessed, using a series of behavioral tests, the reinforcing value associated with optically exciting the upper gut-innervating R-NG neurons. Strikingly, we first observed that fast optogenetic activation of R-NG terminals sustained self-stimulation behavior, the hallmark assay for identifying reward neurons (Olds and Milner, 1954; Schultz, 2015). Specifically, transfected mice produced increasingly greater numbers of operant responses to obtain blue light delivery to NTS; conditioned responses were consistently vigorous, including during subsequent extinction tests (Figure 1F and Movie S1).

During “on-line” place preference tests (in which the laser switch is instantaneously controlled by the animal’s current position), mice mostly stayed at those cage locations paired to laser activation (Figure 1G). Similarly, in flavor conditioning assays, robust preferences were displayed for those initially insipid, non-caloric flavors that had been paired to laser activation (Figures 1H and S1H). The same optical stimulation protocol induced significant reductions in chow (Figure 1I) and lipid (Figures 1J and S1I) intake, demonstrating that food reward is not mutually exclusive to satiation. None of the light-induced effects described above were observed in mice not expressing the optogenetic construct in R-NG (Figures S1J–R).

### **Optical activation of upper gut-innervating vagal sensory neurons induces dopamine release in brain reward pathways**

Dopamine release from *Substantia nigra, pars compacta* (SNc) onto dorsal striatum (DS) is required for behavioral reinforcement by natural rewards as well as by stimulation of brain reward neurons (Crow, 1971; Palmiter, 2008; Phillips et al., 1976; Ungerstedt, 1971). Accordingly, we inquired whether remote excitation of vagal sensory neurons is sufficient to induce the release of dopamine from nigral dopamine neurons onto DS. Using microdialysis sampling coupled to electrochemical detection, we found that optically exciting the upper gut-innervating R-NG neurons significantly increased dopamine levels in DS (Figure 1K), consistent with a role for gut-innervating R-NG neurons in reward. Accordingly, R-NG stimulation modulated neuronal ensemble activity in DS (Figures S1S–V).

In sum, R-NG neurons appear to function similarly to brain reward neurons; namely, R-NG activation sustains self-stimulation, conditions stimulus preferences, and excites brain dopamine cells (Olds, 1976; Schultz, 2015).

### **Laser-induced rewarding and dopaminergic effects are specific to the right nodose ganglion**

In animals similarly injected with the ChR2 construct in the left nodose ganglion (L-NG), overlapping expression of AAVrg-pmSyn1-EBFP-*Cre* and DIO-ChR2-EYFP was equally detected in L-NG neurons (Figure 1L). Counts of *Cre*-transfected cells were comparable in R-NG *v.s.* L-NG (Figure S1A). Regionally restricted expression of EYFP within L-NG (Figure S1W) was consistent with EYFP-positive fibers innervating the upper-gut but not

other organs (Figures S1X–Z). Left nerve recordings also revealed light-locked electrical activity in vagal fibers (Figure 1M) independently of changes in gastric motility (Figure S1AA).

### **Right versus left nodose ganglia modulate distinct brainstem sectors**

We observed conspicuous asymmetries in NG terminal fields in the central nervous system. Specifically, L-NG projects strongly to a posterior part of *area postrema* (AP) and lightly to the NTS (Figure 1N). This is in contrast to R-NG, which projects very substantially to the ventromedial NTS and only lightly to posterior AP (*cf.* Figure 1D). Accordingly, an optic fiber was placed immediately above these L-NG neuronal terminals in AP (Figure 1O). Optical activation of these terminals completely failed to sustain self-stimulation behavior (Figure 1P). Similarly, neither attraction nor aversion was formed upon laser stimulation during on-line place preference tests (Figures 1Q–R). Despite the lack of reinforcement effects, L-NG optical stimulation did induce significant decreases in both chow (Figure 1S) and lipid (Figure 1T) intake. Consistent with the induction of satiation in the absence of rewarding effects, L-NG optical stimulation equally failed to alter striatal dopamine levels (Figure 1U). Overall, these results indicate that right, but not left, NG neurons have privileged access to *Substantia nigra* dopaminergic reward neurons.

To confirm such functional asymmetries, we implanted optical fibers above the AP (in the area innervated by L-NG terminals) in mice injected with ChR2 into the R-NG; conversely, we also implanted optical fibers above the NTS (in the area more extensively innervated by R-NG terminals) in mice injected with ChR2 into the L-NG. In both cases neither behavioral nor dopaminergic effects were detected (Figures S1BB–MM). These results were paralleled by Fos expression analyses (Figure S1G).

### **Targeted nodose terminal fields were gut-specific**

To assess the organ-specificity of the gut terminal fields throughout the solitary complex, we injected a fixed volume of the retrograde *Cre*-carrying construct AAVrg-pmSyn1-EBFP-*Cre* into the upper gut, the heart, the lung or the trachea. In all cases, *Cre*-inducible DIO-ChR2-EYFP was injected into nodose ganglia bilaterally. Analyses revealed a distinct organ-specific map where only gut terminals innervated the ventromedial NTS (Figures 2A–D and S2A–D). This is in agreement with earlier heart and lung terminal maps (Corbett et al., 2005; McGovern et al., 2015). Accordingly, and unlike NG neurons innervating organs such as the lung or heart (Chang et al., 2015), gut-specific activation of neither R-NG nor L-NG caused changes in respiratory or cardiovascular tone (Figures S2E–H). Conversely, stimulation of gut-innervating parasympathetic vagal motor neurons induced gut motility in the absence of any rewarding or dopaminergic effects (Figures S2I–M).

### **Reward remains unaltered upon simultaneous activation of right and left nodose ganglia**

Physiological situations such as feeding may bilaterally stimulate gut terminal fields. This raises the question of whether L-NG activation alters R-NG-induced reward. While it is unfeasible to target both R-NG and L-NG terminals using optical fibers, bilateral nodose activation may be achieved via chemogenetics (Sternson and Roth, 2014). Accordingly, the stomach and duodenum of wild-type mice were transfected with a retrogradely transported,

*Cre*-carrying construct (CAV2-Cre-GFP, Junyent and Kremer, 2015). Then, the *Cre*-inducible, Gs-coupled designer receptor encoded in the construct AAV-hSyn-HA-rM3D(Gs)-IRES-mCherry (Farrell et al., 2013) was bilaterally injected into the NG of these same mice. Employing the Gs-coupled construct is justified by the robust cAMP-induced enhancement of NG neuronal excitability (Ingram and Williams, 1994). This approach allowed for bilateral, upper gut-exclusive excitation of NG neurons and their brainstem targets (Figures 2E–F, S2N–Q).

Administering the designer drug clozapine-N-oxide (CNO) induced the formation of robust place and flavor preferences (Figures 2G–H and S2R), reductions in food intake (Figures S2S–T) and increases in striatal dopamine (Figures 2I and S2U–V). Thus, activating L-NG does not disrupt the rewarding and dopaminergic effects associated with activating R-NG. None of these effects were observed when either CNO or clozapine were injected in mice not carrying the chemogenetic construct (Figures S2W–AA).

### **A polysynaptic neuronal pathway links the right vagal sensory ganglion to dopamine cells**

We next aimed at mapping the central pathways linking vagal sensory ganglia to nigral dopamine neurons. Because nodose ganglia do not contact the midbrain directly, we employed an anterograde transsynaptic viral tracer for mapping vagal outputs. Since NG neurons unconditionally express VGlut2 (Williams et al., 2016), we injected the *Cre*-inducible, transsynaptic Herpes Simplex Viruses 1 strain H129 TK-TT (Lo and Anderson, 2011) into the R-NG of VGlut2-ires-*Cre* mice (Figure 3A).

Forty-eight hours after the injections, infection was restricted to the dorsal vagal complex, including NTS (Figures 3B–C). This pattern was consistent with the ones obtained from injecting the *Cre*-inducible monosynaptic synaptophysin construct AAV8.2-hEF1a-DIO-synaptophysin-EYFP into the R-NG of VGlut2-ires-*Cre* mice (Figure S3A). Seventy-two hours post-injection, infection extended onto NTS targets, including paraventricular hypothalamic nuclei (Figure 3D), in addition to the dorsolateral region of the parabrachial nucleus (PBNdl, Figures 3E and S3B). Ninety-six hours post-injection, a number of regions rostral to PBNdl were infected including the lateral aspect of SNc (Figure 3F). Several infected neurons in SNc were found to be dopaminergic (Figure 3G). A detailed description of infection patterns up to 120hs post-injection is provided in Figure S3B.

*The dorsolateral parabrachial nucleus links the right vagal sensory ganglion to Substantia nigra* Consistent with previous reports (Coizet et al., 2010), injection of a retrograde dye into SNc predominantly revealed profuse labeling in PBNdl (Figure S3C). Critically, labeling was restricted to the site where herpes infection was observed (excluding therefore the externolateral parabrachial nucleus, PBNel, Figure S3C). No retrograde labeling was detected in the dorsal vagal complex. We thus hypothesized that PBNdl links the vagal central pathways to SNc. Since VGlut2 is enriched in the lateral parabrachium (Kaur et al., 2013), we more specifically predicted that vagal sensory information reaches SNc via an excitatory relay in PBNdl. We introduced the viral construct AAV-flex-taCasp3-TEVp (Yang et al., 2013), which induces *Cre*-dependent caspase expression, bilaterally into the PBNdl of VGlut2-ires-*Cre* mice. After three weeks, we injected the R-NG of these same mice with the H129 TK-TT construct. Despite infection of the dorsal vagal complex and their

hypothalamic targets, labeling was completely abolished in both PBNdl and SNc (Figure S3D). Remarkably, H129 TK-TT injections into the L-NG produced no labeling in either PBNdl or SNc (Figure 3H–K, S3E). The latter is consistent with the optogenetic data revealing right nodose ganglion-specific effects.

### **The source of vagal sensory inputs to dopamine cells is the upper gut**

We next aimed at determining whether gut-innervating nodose neurons are necessary and sufficient sources of vagal inputs to SNc. We again transduced the stomach and duodenum of wild-type mice with the retrograde construct AAVrg-pmSyn1-EBFP-*Cre*, and after three weeks H129 TK-TT was injected in the R-NG of these mice (Figure 3L). We again observed infection of both PBNdl and lateral SNc dopaminergic cells (Figures 4M–R and S4F), demonstrating that transsynaptic labeling from upper gut-innervating R-NG neurons is sufficient to induce labeling in SNc.

Conversely, we also induced selective vagal deafferentation of the gut previous to introducing the transsynaptic virus into R-NG. This was achieved by injecting the neurotoxin saporin conjugated to cholecystokinin (CCK-SAP, Diepenbroek et al., 2017) into the R-NG of VGlut2-ires-*Cre* mice. The R-NG of these mice was then injected with H129 TK-TT. After vagal deafferentation of the gut, labeling was restricted to the dorsal motor nucleus of the vagus (Figure S3G).

### **Separate regions of the lateral parabrachial nucleus respond to aversive vs. rewarding stimuli**

The lateral parabrachial region is known to mediate avoidance behaviors, including responses to visceral malaise (Carter et al., 2013). This is in principle inconsistent with our results suggesting a lateral parabrachial relay for vagus-induced reward. This apparent contradiction led us to hypothesize that the lateral parabrachial complex contains separate subnuclei that act to mediate reward *vs.* avoidance behaviors.

We used Fos induction to map lateral parabrachial responses to aversive *vs.* rewarding visceral stimuli. Specifically, we compared Fos responses to systemic injections of the vagus-mediated digestive peptide cholecystokinin (CCK, Smith et al., 1985) *vs.* to malaise-inducing lithium chloride (LiCl). Importantly, CCK and LiCl doses were titrated so that both treatments produced a statistically equivalent, ~50% reduction in food intake (Figure 4A). Despite producing the same behavioral outcome, injections of these doses of CCK and LiCl induced highly dissimilar Fos expression patterns in the lateral parabrachium: whereas LiCl responses were restricted to the externolateral aspect (PBNel), CCK responses were circumscribed to dorsolateral and, to a lesser extent, medial regions (PBNdl and PBNm, Figures 4B–E). Thus, neuronal responses to CCK, but not to LiCl, overlapped with the herpes-infected right vagus-recipient parabrachial areas.

CGRP-positive neurons of the lateral parabrachium are critical mediators of avoidance behaviors (Carter et al., 2013). We therefore hypothesized that Fos induced by LiCl, but not by CCK, overlaps with CGRP expression. Double immunostaining confirmed our assumption that LiCl-responsive neurons amalgamate with CGRP-positive neurons within

PBNel, whereas most CCK-responsive neurons are CGRP-negative cells located more dorsally within PBNdl (Figures 4F–G and S4A–F).

### ***Vagus-recipient parabrachial neurons preferentially Substantia nigra***

Based on the above, we predicted that PBNdl and PBNel should send their efferents to separate downstream targets. To obtain small injections restricted to parabrachial subnuclei, we injected the sensitive anterograde tracer *Phaseolus vulgaris* leucoagglutinin (PHA-L) into PBNdl vs. PBNel.

We found that PHA-L injections restricted to PBNdl – where both CCK-responsive and R-NG-transsynaptic targets are located (*cf.* Figure 3E) – resulted in a dense terminal field in the midbrain dopaminergic complex, including SNc (Figures 4H–I and S4H–I). Importantly, concomitant injections of the retrograde tracer FluoroGold into DS (Figure S4G) revealed that PBNdl terminal fibers and DS-projecting neurons are in register in SNc (Figure 4J), suggesting the existence of a parabrachio-nigro-striatal pathway.

Strikingly, PHA-L injections into PBNel resulted in virtually no labeling in dopaminergic midbrain regions (Figures 4K and S4J). In contrast, these PBNel injections resulted in a dense terminal field in the caudal lateral and capsular parts of the central amygdaloid nucleus (CeL/C, Figure S4K). Consistently, retrograde tracer injections into CeL/C resulted in a robust labeling that was restricted to PBNel (Figures S4L–M). Accordingly, Fos responses to LiCl were restricted to the amygdalar targets of PBNel (Figure S4N).

To assess the cell-type specificity of parabrachio-nigral targets, we transfected the SNc of both DAT-ires-*Cre* and VGat-ires-*Cre* mice with the *Cre*-inducible, retrograde pseudotyped monosynaptic rabies virus SAD G-GFP (Figure 4L, Wickersham et al., 2007). We observed dense, rabies-infected fields in PBNdl, but not in the PBNel, of both DAT-ires-*Cre* and VGat-ires-*Cre* mice (Figures 4M–N). The rabies retrograde patterns further demonstrate that CGRP-positive neurons (mostly restricted to PBNel) do not project to SNc (Figures 4M–N). No retrograde rabies infection was observed in the dorsal vagal complex, confirming that the latter does not relay vagal afferents directly to SNc (Figure S4O–T). In contrast, SAD G-GFP injected into the PBNdl of VGlut2-ires-*Cre* mice revealed dense retrograde labeling in the NTS field innervated by R-NG afferents (Figures S4U–V). Overall these results support a circuit model in which VGlut2-positive neurons in PBNdl act as an obligatory relay linking right nodose gut signals and SNc. Of note, AgRP-positive terminal fields were detected throughout both LiCl- and CCK-responsive areas (Figure S4W). This may account for how GABAergic AgRP neurons counteract the inhibitory actions of both CCK and LiCl (Wu et al., 2012). Finally, the anatomical findings were mirrored by functional studies revealing opposing dopamine responses to CCK vs. LiCl (Figures 4O–S).

### **Remote stimulation of the parabrachio-nigral pathway induces reward and dopamine release**

The labeling studies above suggest that parabrachio-nigral, but not parabrachio-amygdalar, projecting neurons mediate the rewarding and dopaminergic effects of vagal excitation. If our model is correct, activation of PBNdl->SNc terminals should recapitulate the effects

observed upon remote stimulation of gut-innervating R-NG neurons. In contrast, activation of PBNel->CeL/C terminals should elicit avoidance behavior.

Injection of AAV8.2-hEF1a-DIO-synaptophysin-EYFP into the PBNdl of VGlut2-ires-*Cre* mice revealed a substantial terminal field in SNc, especially in the vagus-targeted lateral SNc (Figure 5C). Slice electrophysiological recordings confirmed robust excitation of PBNdl VGlut2-neurons by blue light pulses upon injection of *Cre*-inducible *Channelrhodopsin2* into the PBNdl of VGlut2-ires-*Cre* mice (Figures 5B, 5D-E).

Optic fibers were then placed above PBNdl neuronal terminals in SNc (Figure 5A). In striking similarity to optogenetically exciting R-NG terminals, PBNdl->SNc activation sustained self-stimulation behavior at comparable response levels (Figure 5F and Movie S2). Likewise the gut-to-brain optogenetics results, transfected mice produced increasingly greater numbers of operant responses to obtain blue light delivery to SNc; conditioned responses were consistently vigorous, including during subsequent laser-off extinction tests.

Additionally, during “on-line” place preference tests (in which the laser switch is instantaneously controlled by the animal’s current position), mice mostly stayed at those cage locations paired to laser activation (Figure 5G and Movie S3). Similarly, in flavor conditioning preference tests, robust preferences were displayed for those initially insipid, non-caloric flavors that had been paired to laser activation (Figures 5H and S5A). Finally, PBNdl->SNc optical activation induced robust satiety during both chow and lipid intake (Figures 5I and S5B-C).

Interestingly, injection of the *Cre*-inducible monosynaptic synaptophysin construct into PBNdl of VGat-ires-*Cre* mice failed to label terminal fields in SNc. On the other hand, similar injections into the PBNel of VGat-ires-*Cre* mice revealed a dense GABAergic termination field in PBNdl (Figures S5D-F). Optical stimulation of these VGat-neurons, which do not project to SNc (Figures S5G-H), produced strong place avoidance during on-line place preference tests as well reductions in intake (Figures S5I-J), further demonstrating that the rewarding effects of stimulating PBNdl are mediated by glutamatergic projections to SNc.

Also consistent with the effects of stimulating right vagal sensory neurons, optical PBNdl->SNc activation induced the dopamine release onto DS (Figure 5J). Altogether, these results indicate that optically activating PBNdl->SNc terminals recapitulate the dopaminergic and behavioral effects of optically activating R-NG neurons. In contrast, we examined the effects associated with stimulating the PBNel->CeL/C pathway (Carter et al., 2013). In a pattern that was strikingly opposed to PBNdl->SNc, PBNel->CeL/C optogenetic activation produced place and flavor avoidance (Supplemental Figures S5K-R and Movie S4).

### **The right-vagus-parabrachio-nigrostriatal pathway is required for nutrient sensing**

We confirmed the existence of a right-vagus-parabrachio-nigrostriatal by injecting a retrogradely transported, polysynaptic pseudo-rabies viral construct (Banfield et al., 2003) bilaterally into DS (Figure 6A). We observed dense labeling in the right, but not left, NG (Figures 6B-C). Retrogradely labeled brain regions included the medial NTS and PBNdl

upper gut terminal sites (Figures 6D–F and S6A–E). Accordingly, behavioral responses to CCK were equally abolished by striatal dopamine receptor antagonism (Figure 6G); right, but not left, gut vagal deafferentation (Figure 6H); and targeted lesions to the parabrachio-nigral pathway (Figure 6I). The behavioral findings were mirrored by Fos expression patterns (Figures 6J–L). A series of loss-of-function studies demonstrate that vagal and parabrachio-nigral ablations abolish reward and dopamine release while preserving aversion (Figures S6F–LL).

## Discussion

Our findings reveal the existence of a neuronal population of “reward neurons” amid the sensory cells of the right vagus nerve. Formally, these vagal sensory neurons operate under the same constraints attributed to reward neurons of the central nervous system (Olds, 1976; Schultz, 2015). Thus, gut-innervating right nodose ganglion neurons link peripheral sensory cells to the previously mapped populations of reward neurons in brain (Crow, 1973; Olds, 1976; Schultz, 2015).

Our findings more specifically imply that food reinforcement and satiation should not be considered mutually exclusive physiological processes. Conceptually, our results appear to reconcile the intracranial self-stimulation phenomenon with the earliest view of rewards as “drive inhibitors” (Hull, 1943). Consistently, activating the hypothalamic AgRP-positive “drive” neurons counteract parabrachium-mediated satiety (Campos et al., 2016) while conveying negative valence (Betley et al., 2015). Interestingly, recent findings do show in fact that stimulating the gut-brain axis with nutrients suppresses AgRP-neuronal activity (Beutler et al., 2017; Su et al., 2017), raising the possibility that vagal satiating/rewarding signals inhibit AgRP-elicited drives.

Related to the above, we do note that separate groups of nodose ganglia neurons have previously been associated with different alimentary functions (Altschuler et al., 1989; Shapiro and Miselis, 1985), including chemosensory *vs.* mechanosensory signaling (Williams et al., 2016). These findings lead to the hypothesis that nodose neurons mediating reward (*i.e.* right nodose neurons) may be particularly sensitive to nutritive signals whereas those inducing satiation independently of reward (*e.g.* left nodose neurons) may preferentially display responses to mechanical distention. This possibility is suggested by the striking specificity with which the right nodose ganglion controls the effects of cholecystokinin on appetite. Consistently, we found that the right nodose ganglion polysynaptically linked to dorsal striatum dopamine release. Overall, our data revealed a gut-originated ascending pathway consisting of the right nodose, the parabrachio-nigral pathway, and its targets in dorsal striatum, where each node was found to be required for CCK actions on appetite. Divergent stimulus selectivity in left *vs.* right nodose ganglia may ultimately rationalize such striking asymmetry in vagal central pathways.

As mentioned, we identified a dorsolateral parabrachio-nigral pathway that is critical for the expression of reward behaviors mediated by gut vagal afferents. Transsynaptic labeling of right vagal origin targeted this pathway, which not only responded to digestive intestinal hormones, but also induced reward behaviors when stimulated. While consistent with

previous studies showing that CCK may induce flavor preferences (Perez and Sclafani, 1991), these findings contrast with the notion that CCK engages CGRP-positive neurons of the externolateral parabrachial nucleus (Carter et al., 2013). While these authors do in fact observe that CCK-induced activation of CGRP-positive neurons likely derives from severe forms of satiety, their subsequent studies also suggest that CGRP-positive neurons may participate in more physiological forms of CCK-induced satiation (Campos et al., 2016). Therefore, future designs must more precisely explore parabrachial activation in response to gut hormone administration under a variety of physiological conditions.

Cervical vagal stimulation is an approved treatment for refractory major depression (Carreno and Frazer, 2017). Interestingly, the stimulator is commonly implanted on the left side to avoid the cardiac complications elicited by electrically exciting the sinoatrial node (Howland, 2014). Our results on the other hand suggest that positive affective states may be more efficiently induced by means of stimulating the right vagus nerve. Accordingly, one possible approach around cardiac complications may be implanting the stimulator on vagal nerve segments located at the vicinity of the upper gut. Future vagus nerve stimulation trials coupled to measurements of human striatal dopamine release may determine the extent to which upper gut vagal excitation enhances dopamine signaling within reward pathways of depressed patients.

## STAR Methods

### Contact for Reagents and Resource Sharing

Further information and requests for reagents should be directed to, and will be fulfilled by the Lead Contact Ivan E de Araujo <IAraujo@jbpierce.org, ivan.araujo@yale.edu>.

### Experimental Model and Subject Details

All experiments presented in this study were conducted according to the animal research guidelines from NIH and were approved by the Institutional Animal Care and Use Committee of The J.B. Pierce Laboratory.

**Experimental Animals**—A total of 247 adult male mice were used. Strain details and number of animals in each group are as follows:

183 C57BL/6J (Jackson Laboratories stock #000664)

9 VGat-ires-*Cre* (Slc32a1<sup>tm2(cre)Low1</sup>/J (Jackson Laboratories stock #016962)

40 VGlut2-ires-*Cre* (Slc17a6<sup>tm2(cre)Low1</sup>/J (Jackson Laboratories stock #016963)

2 Dat-ires-*Cre* (Slc6a3<sup>tm1.1(cre)Bkmn</sup>/J (Jackson Laboratories stock #006660)

2 Dat-ires-*Cre* × Ai14 = Dat-ires-*Cre* (Slc6a3<sup>tm1.1(cre)Bkmn</sup>/J (Jackson Laboratories stock #006660) × Ai14 (B6.Cg-Gt(ROSA)26Sortm14(CAG-tdTomato)Hze/J (Jackson Laboratories stock #007914)

1 *Agrp-ires-Cre* × *Ai34D* = *Agrp-Cre* (*Agrpt*<sup>m1(cre)Low</sup> (Jackson Laboratories stock #012899) × *Ai34D* (B6;129S-Gt(ROSA)26Sor<sup>tm34.1(CAG-Syp/tdTomato)Hze/J</sup> (Jackson Laboratories stock #012570) 10 *Ai14* (B6.Cg-Gt(ROSA)26Sor<sup>tm14(CAG-tdTomato)Hze/J</sup> (Jackson Laboratories stock #007914)

All mice used in experiments were individually housed under a 12 hr light/dark cycle. At the time of the experiments, animals were 8–20 weeks old. Animals weighed approximately 25–28 grams. All animals were used in scientific experiments for the first time. This includes no previous exposures to pharmacological substances or altered diets. Health status was normal for all animals.

## Method Details

The following provides details on viral injections and fiber/array implantation for each mouse strain. In all cases, preoperative analgesia: 0.05mg/Kg Buprenorphine (*s.c.*); anesthetic: 2% Isoflurane throughout; postoperative analgesia: 5mg/Kg Carprofen (*s.c.*) twice per day for consecutive 3 days. All surgeries were processed having the animals placed on a heated pad (CMA 450; Harvard Apparatus, Holliston, MA), and allowed to recover under infrared heat until they chose to reside in the unheated side of the cage.

**Peripheral organs viral injections**—The viral constructs (*CAV2-Cre-GFP* or *AAVrg-pmSyn1-EBFP-Cre*) were loaded into a Nanofil™ 36G beveled needle (World Precision Instruments, Sarasota, FL) and Silflex™ tubing (World Precision Instruments, Sarasota, FL), connected to a Nanofil™ 10 µl syringe (World Precision Instruments, Sarasota, FL) and mounted on a Pump 11 Elite Nanomite (Harvard Apparatus, Holliston, MA). Upper gut: Multiple 0.03 µl injections were made at 0.01 µl/s into each submucosal puncture. Each animal received a total volume of 1µl in the stomach, duodenum and proximal jejunum. Myocardium: a total volume of 1µl of viral construct was injected into the ventricular muscle through the central tendon of diaphragm. Pulmonary lobe: a total volume of 1µl of viral construct was injected into the right pulmonary lobe through central tendon of diaphragm. Trachea: a total volume of 0.5µl of viral construct was injected into the wall of the upper trachea between larynx and clavicle.

**Nodose ganglia injections**—The vagus nerve was separated from the carotid artery with a Spinal Cord Hook (Fine Science Tools, Foster City, CA) until the nodose ganglion became accessible. Viral aliquots (*AAV-hSyn-DIO-rM3D(Gs)-mCherry*; *AAV-EF1a-DIO-EYFP*; *AAV5-EF1a-DIO-hChR2(H134R)-EYFP*; *AAV5-flex-taCasp3-TEVp*; H129 TK-TT) or chemicals (CCK-SAP (250ng/µl; IT-31) or SAP (250ng/µl; IT-21)) were loaded into a Nanofil™ 36G beveled needle (World Precision Instruments, Sarasota, FL) and Silflex™ tubing (World Precision Instruments, Sarasota, FL). For each nodose ganglion, a total 0.5µl volume was delivered into two sites, rostral and caudal to the laryngeal nerve branch, at 0.2ul/min using a Nanofil™ 10 µl syringe (World Precision Instruments, Sarasota, FL) mounted on a Pump 11 Elite Nanomite (Harvard Apparatus, Holliston, MA).

**Stereotaxic viral injections and optical fiber implantation**—The following provides details on viral injections for each mouse strain. In all cases, injections were

performed with a Hamilton 1.0 $\mu$ L Neuros Model 7001KH syringe, at a rate of 0.02 $\mu$ L/min. In what follows, and for each mouse strain, we first list the viral construct injected, then the relevant stereotaxic coordinates for the injections are described. When applicable, the relevant stereotaxic coordinates for optical fibers implantation are described. Optical fibers were obtained from Doric Lenses, Inc. (Canada) the outer diameter of which is 240 $\mu$ m; core diameter is 200 $\mu$ m; numerical aperture is 0.22. Stereotaxic coordinates are with respect to *bregma*, according to a standardized atlas of the mouse brain (Keith Franklin & George Paxinos, *The Mouse Brain in Stereotaxic Coordinates*, Compact 3rd Edition, Academic Press, 2008).

Mouse strain **C57/BL6J**

Injection type *Upper gut-AAVrg-Cre*

Viral construct AAVrg-pmSyn1-EBFP-Cre (1  $\mu$ L)

**These same animals were injected with Cre-dependent viral constructs in Nodose ganglia or dorsal motor nucleus of the vagus.:** Injection type Nodose ganglia

Viral construct

AAV-hSyn-DIO-rM3D(Gs)-mCherry; AAV-EF1a-DIO-EYFP; AAV5-EF1a-DIO-hChR2(H134R)-EYFP; AAV5-flex-taCasp3-TEVp (0.5  $\mu$ L)

Opto fiber Coordinates:

NTS: AP:-7.5mm, ML:  $\pm$ 0.3mm, DV -5.0mm.

AP: AP:-7.6mm, ML:  $\pm$ 0mm, DV -4.8mm

Injection type *dorsal motor nucleus of the vagus*

Viral construct AAV5-EF1a-DIO-hChR2(H134R)-EYFP (0.3  $\mu$ L)

Control viral construct AAV-EF1a-DIO-EYFP (0.3  $\mu$ L)

Viral injection Coordinates:

AP:-7.5mm, ML:  $\pm$ 0.3mm, DV -5.5 ~-5.3mm.

Opto fiber Coordinates:

DMV: AP:-7.5mm, ML:  $\pm$ 0.3mm, DV -5.2mm.

Mouse strain **Ai14**

Injection type *SNc-AAVrg-Cre*

Viral construct AAVrg-pmSyn1-EBFP-Cre

AP: -3.6mm, ML:  $\pm 1.5$ mm, DV -4.0mm ~ -4.2mm. 0.3 $\mu$ L each side.

**These same animals were injected with Cre-dependent Caspase in PBNdl: Viral construct AAV5-flex-taCasp3-TEVp**

Control viral construct AAV-EF1a-DIO-EYFP

AP: -5.3mm, ML:  $\pm 1.5$ mm, DV -4.0mm ~ -4.2mm. 0.3 $\mu$ L each side.

Mouse strain **VGlut2-Cre**

Injection type PBNdl-DIO-ChR2, opto fibers in SNc

Viral construct AAV5-EF1a-DIO-hChR2(H134R)-EYFP

AP: -5.3mm, ML:  $\pm 1.5$ mm, DV -4.0mm ~ -4.2mm. 0.3 $\mu$ L each side.

Opto fiber Coordinates: AP: -3.6mm, ML:  $\pm 1.5$ mm, DV -4.0mm.

Injection type PBNeI-DIO-ChR2, opto fibers in CeL/C

Viral construct AAV5-EF1a-DIO-hChR2(H134R)-EYFP-WPRA-pA

AP: -5.3mm, ML:  $\pm 1.6$ mm, DV -4.2mm ~ -4.5mm. 0.3 $\mu$ L each side.

Opto fiber Coordinates: AP: -1.6mm, ML:  $\pm 2.7$ mm, DV -4.5mm.

Mouse strain **VGat-Cre**

Injection type PBNeI-DIO-ChR2, opto fibers in PBNeI

Viral construct AAV5-EF1a-DIO-hChR2(H134R)-EYFP-WPRA-pA

AP: -5.3mm, ML:  $\pm 1.6$ mm, DV -4.2mm ~ -4.5mm. 0.3 $\mu$ L each side.

Opto fiber Coordinates: AP: -5.3mm, ML:  $\pm 1.6$ mm, DV -4.0mm.

## **Anatomical tracing studies**

### **Anterograde tracing using Phaseolus vulgaris leucoagglutinin (PHA-L)**

**PBN-PHA-L:** 2.5% PHA-L in phosphate buffer (pH 7.4) was injected unilaterally by iontophoresis by passing a positive-pulsed (7 seconds on/off) current (4.5  $\mu$ A for 13–20 min) through a glass micropipette of ~ 15  $\mu$ m of internal tip diameter. For the stereotaxic approach to the PBN, the caudal pole of the inferior colliculus was used as anteroposterior landmark. Coordinates AP: 0.6 mm, ML: 1.3–1.5 mm, DV: 2.6 mm

**Anterograde tracing using Cre-dependent synaptophysin expression:** Anatomical markers in all images shown are according to standardized atlases of the adult mouse brain. The following mouse strains and injections were used for assessment of cell-specific anterograde and retrograde projections. Injections were performed unilaterally. The viral

construct used was the Cre-dependent AAV8.2-hEF1a-DIO-synaptophysin-EYFP, which allows for analysis of Cre-inducible synaptophysin expression.

Mouse strain **VGlut2-Cre**

Injection type PBNdl- synaptophysin

Injection Coordinates

AP:-5.3mm, ML:  $\pm 1.5$ mm, DV -4.0mm  $\sim$ -4.2mm. 0.3 $\mu$ L

Mouse strain **VGlut2-Cre**

Injection type Right nodose ganglia - synaptophysin 0.3 $\mu$ L

Mouse strain **VGat-Cre**

Injection type PBNel- synaptophysin

Injection Coordinates

AP:-5.3mm, ML:  $\pm 1.6$ mm, DV -4.2mm  $\sim$ -4.5mm. 0.3 $\mu$ L

Retrograde tracing

CeL/C-FluoroGold

1% FG 0.05 $\mu$ L was injected unilaterally, speed 0.05 $\mu$ L/20min. Coordinates AP:-1.6mm, ML: 2.7mm, DV -4.8mm.

**DS-FluoroGold:** 2% FG in saline was injected unilaterally by iontophoresis by passing a positive-pulsed (7 seconds on/off) current (1.5  $\mu$ A for 6 min) through a glass micropipette of 20–25  $\mu$ m of internal tip diameter. Two injections 0.6 mm apart were made along the dorsoventral axis. Coordinates AP: 1 mm, ML: 1.4 mm, DV: 2.2 mm and 2.8 mm.

**Snc-RetroBeads:** 0.3 $\mu$ L RetroBeads was injected unilaterally, speed 0.02 $\mu$ L/min. Coordinates AP:-3.6mm, ML: 1.6mm, DV: -5.2mm  $\sim$ -5.4mm.

Retrograde tracing using Cre-dependent pseudo-typed rabies virus expression

Mouse strains **VGat-Cre, Dat-Cre, Dat-Cre $\times$ tdTomato, VGlut2-Cre**

For starter cells in SNc (AP:-3.6mm, ML:  $\pm 1.6$ mm, DV: -5.2mm  $\sim$ -5.4mm) or PBNdl (AP:-5.3mm, ML:  $\pm 1.5$ mm, DV -4.0mm  $\sim$ -4.2mm), AAV5-CA-FLEX-RG was unilaterally injected at 0.3 $\mu$ L. Two weeks afterwards SAD- G-GFP 0.3 $\mu$ L was injected on the same site. Seven days later, the tissue were collected and then analyzed.

**Histological procedures**—Mice were deeply anesthetized with a ketamine/xylazine mix (400 mg ketamine + 20 mg xylazine kg body weight<sup>-1</sup> I.P.). All animals were perfused with filtered saline, followed by 4% paraformaldehyde. Following perfusion, brains were left in

4% paraformaldehyde for 24 hours and then moved to a 20% sucrose solution in 0.02 M potassium phosphatebuffer (KPBS, pH 7.4) for 2 days. Brains were then frozen and cut into four series 40  $\mu$ m sections with a sliding microtome equipped with a freezing stage. To identify fiber and electrode locations, relevant sections were identified and mounted on slides. Sections were then photographed under bright field and fluorescence. For Herpes Simplex Viruses visualization, 3 or 4 or 5 days after viral injection, mice were perfused and brains cut at 40 $\mu$ m. The tdTomato signal was amplified with Rabbit-anti-mCherry (Abcam, ab167453, 1:500) followed by TRITC-conjugated affinipure Goat anti-Rabbit (IgG (H+L) 111-025-144, Jackson Immuno, 1:200). For Cre-induced rM3D(Gs)-mCherry and hChr2-EYFP visualization, 4 weeks after viral injection, mice were perfused, nodose ganglia and brain were collected and cut at 40 $\mu$ m. The mCherry signal was amplified with Rabbit-anti-mCherry (Abcam, ab167453, 1:500) followed by TRITC-conjugated affinipure Goat anti-Rabbit (IgG (H+L) 111-025-144, Jackson Immuno, 1:200). The EYFP signal was amplified with Goat anti-GFP antibody (FITC), (ab6662, Abcam, 1:500). For synaptophysin visualization, 4 weeks after viral injection, mice were perfused and brains cut at 40 $\mu$ m. The GFP signal was amplified with Goat anti-GFP antibody (FITC), (ab6662, Abcam, 1:500). For verifying the extension of caspase-induced lesions, slices were incubated with Alexa Fluor® 647 recombinant rabbit monoclonal anti-Neuronal Nuclei (NeuN, Abcam ab190565, 1:500) antibody. For Tyrosine Hydroxylase visualization via immunofluorescence, slices were incubated with chicken polyclonal to Tyrosine Hydroxylase antibody (ab76442, Abcam, 1:500), followed by Alexa Fluor® 488 conjugated affinipure goat anti-chicken (IgY (H&L), ab150169, Abcam, 1:200). For CGRP visualization, slices were incubated with Goat polyclonal to CGRP (ab36001, Abcam, 1:500), followed by FITC-conjugated affinipure Donkey Anti-Goat (IgG (H+L) 705-095-147, Jackson Immuno, 1:200) or TRITC-conjugated affinipure Donkey Anti-Goat (IgG (H+L) 705-025-147, Jackson Immuno, 1:200). For FluoroGold and RetroBeads experiments, seven days after injections animals were perfused as above and brains sliced in 40 $\mu$ m sections. For visualization of rabies expression, seven days after the rabies injections, animals were perfused and expression was observed in coronal sections at ~160  $\mu$ m intervals. Visualized cells were overlaid on a mouse brain atlas template.

In experiments using Phaseolus vulgaris leucoagglutinin or Phaseolus vulgaris leucoagglutinin in combination with FluoroGold, after a survival of 5–10 days the animals were perfused as above and the brains sectioned at 30  $\mu$ m. The sections were processed with a rabbit anti-PHA-L (1:5000; Dako, Carpinteria, CA) or with a rabbit anti-FG (1:10000; Bioscience Research Reagents, Temecula, CA) by using the ABC technique (Vectastain, Elite ABC kit 1:400; Vector). The peroxidase reaction product was revealed with the glucose oxidase procedure and the metal-free 3,3'-diaminobenzidine tetrahydrochloride (DAB) as the chromogen. An osmium tetroxide treatment was used to enhance the visibility of the labeling. An adjacent series of sections was stained for thionin. For the simultaneous detection of PHA-L-labeled fibers and tyrosine hydroxylase (TH)-positive mesencephalic neurons, sections were first processed for PHA-L immunohistochemistry by using the nickel intensification method and then immunostained for TH (with a mouse anti-TH 1:5000; ImmunoStar, Hudson, WI) by using the metal-free DAB as the chromogen. A similar procedure was adopted for the simultaneous detection of PHA-L-labeled fibers and FG-

positive neurons in the nigral complex, but in this case, a goat anti-PHA-L (1:4000; Vector) and a rabbit anti-FG (1:10000; Chemicon) were used as primary antibodies.

**c-Fos measurements**—For determining the effects of chemogenetic, CCK or LiCl stimulation on brainstem neuronal activity, 90 minutes after the appropriate stimulation, mice were sacrificed and perfused as described before. To visualize Fos immunoreactivity, either the ABC/DAB procedure or immunofluorescence was used. Briefly, brain sections was incubated with Rabbit Anti-c-Fos antibody (Abcam (ab190289), 1:10000), followed with Biotinylated Goat Anti-Rabbit IgG Antibody (BA-1000, Vector Laboratories, 1:200), then reacted with avidin-biotin-peroxidase complex (“ABC” method, Vectastain Elite ABC kit, Vector Laboratories, 1:200). A nickel diaminobenzidine (Nickel-DAB) glucose oxidase reaction was used to visualize Fos-like immunoreactive cells. To visualize Fos via immunofluorescence, slices were incubated with Rabbit Anti-c-Fos antibody (Abcam (ab190289), 1:2000), followed by TRITC-conjugated affinipure goat anti-rabbit (IgG (H+L) 111-025-144, Jackson Immuno, 1:200) or FITC-conjugated affinipure goat anti-rabbit (IgG (H+L) 111-095-144, Jackson Immuno, 1:200). Fos expression was analyzed and quantified as follows: Coronal sections at ~160  $\mu$ m intervals were photographed at 10 $\times$  magnification and montaged with Adobe Photoshopto to preserve anatomical landmarks. Fos+ neurons were counted with ImageJ on each slice and expressed as the cumulative sum of Fos+ neurons within the relevant regions for each animal.

**Whole-Mount Immunostaining and Gut Tissue Clearing**—The animals were anesthetized and perfused with saline and 1%PFA. The upper gut, heart and lung were dissected, opened and cleaned in a 1%PFA solution. Then the attached connective tissues were removed. After 24h fixation with 4% PFA at 4°C, the tissues were washed with PBS for 1hr, which was then repeated twice. Tissues were then dehydrated at room temperature in a series of methanol/ddH<sub>2</sub>O solutions (20%, 40%,60%,80%,100%,100%), 30 min for each concentration. The tissue was next imbedded with a mixture of dichloromethane (Sigma)/methanol (2 volumes/1 volume) for 3hr, and then with 100% dichloromethane for 15 min, twice. The tissue was then transferred to a cover-glass bottomed chamber and then finally cleared with 100% dibenzyl-ether (Sigma) for 1 hr twice, and prepared for confocal imaging.

**Surgical Procedure for Implantation of Gastric Catheters and Microdialysis Guiding Cannulae**—Once animals had been anesthetized, a midline incision was made into the abdomen. The stomach was exteriorized through the midline incision and a purse string suture was placed in its non-glandular region, into which the tip of MicroRenathane tubing (Braintree Scientific Inc., Braintree, MA) was inserted. The purse string was tightened around the tubing, which was then tunneled subcutaneously to the dorsum via a small hole made into the abdominal muscle; a small incision to the dorsum between the shoulder plates was then made to allow for catheter exteriorization. Incisions were sutured and thoroughly disinfected and the exterior end of the catheter plugged. Immediately after the above procedure, the animal was placed on a stereotaxic apparatus (David Kopf) under constant flow of ~2% isoflurane anesthesia and a circular craniotomy was drilled at AP = 1.5 mm, ML =  $\pm$ 1.5 mm implantation of a guide cannulae [DV = -1.5 mm from brain surface]

for posterior insertion of a microdialysis probe into the dorsal aspect of the striatum (final probe tip positions [DV = -3.5 mm from brain surface]).

**Dopamine measurements during intra-gastric infusions**—Previous to, during, and after intra-gastric infusions (rate: 30 $\mu$ L/min; total volume: 0.6mL), microdialysate samples from mildly food-deprived awake mice freely moving in their home cages were collected, separated and quantified by HPLC coupled to electro-chemical detection methods (“HPLC-ECD”). Briefly, after recovery from surgery, a microdialysis probe (2mm CMA-7, cut off 6kDa, CMA Microdialysis, Stockholm, Sweden) was inserted into the dorsal striatum through the guide cannula (the corresponding CMA-7 model). After insertion, probes were connected to a syringe pump and perfused at 1.2 $\mu$ L/min with artificial CSF (Harvard Apparatus). After a 40 min washout period and a subsequent 30 min pre-intake baseline sampling, dialysate samples were collected every six minutes and immediately manually injected into a HTEC-500 HPLC unit (Eicom, Japan). Analytes were then separated via an affinity column (PP-ODS, Eicom), and compounds subjected to redox reactions within an electro-chemical detection unit (amperometric DC mode, applied potential range from 0 to ~2000 mV, 1mV steps). Resulting chromatograms were analyzed using the software EPC-300 (Eicom, Japan), and actual sample concentrations were computed based on peak areas obtained from a 0.5pg/ $\mu$ L dopamine standard solution (Sigma) and expressed as % changes with respect to the mean dopamine concentration associated with the baseline (i.e. pre-infusions) sampling period. Microdialysis sessions involving optical stimulation were performed identically as above, except that after collecting the baseline, laser source was turned on for 12min at intermittent ON/OFF intervals of 30s. Locations of microdialysis probes were confirmed histologically. All experiments were performed on animals clearly alert and moving naturally in their home cages.

**Brain infusions of dopamine antagonists**—Cannulae for striatal infusions were obtained from Plastics One (Roanoke, VA). The D1/D2 dopamine receptor antagonist flupenthixol (Sigma) was infused bilaterally into the dorsal striatum at coordinates AP = 1.5 mm, ML =  $\pm$ 1.5 mm DV = -2.5 at 15 $\mu$ g/0.5 $\mu$ L/hemisphere. The drug was prepared in aCSF (used as vehicle control) 5 minutes previous to the 1h-long oral intake tests.

**Electromyogram electrodes, recordings and analyses**—First, two twisted Formvar-Insulated Nichrome Wires (Diameter: Bare 0.002 inch. A-M system) were covered with polyethylene tubing (PE20, 0.15”  $\times$  0.45”, Braintree scientific). The tips of the nichrome wires were bared and exposed. One bare wire tip was soldered to a Male Miniature Pin Connector (520200, A-M Systems). The other bare wire tip was inserted through a 30G needle, and the tip bent and used for the implants into the stomach. For implants, the needle was then used for insertion of the wire into the stomach via a small hole made into the abdominal muscle, with the bare wire hooked into the stomach. A suture was used to fix the wire in place. In order to verify the efficacy of the recordings, at the end of each session animals were administered the gut motility-inducing drug metoclopramide hydrochloride (10mg/kg i.p.). Recordings were performed using the electromyogram module of a multichannel acquisition processor (Tucker-Davis Technologies, 3052Hz sampling rate). The male pin connector was attached to the female connector, which had been soldered to a

recording headstage. Laser pulses timestamps were synchronized to the recordings via external TTL pulses into the TDT system. EMG signals from the stomach were recorded simultaneously to vagal nerve recordings in the same animals.

**In vivo vagus nerve trunk recordings**—The vagus nerve trunk was separated from the carotid artery with a Spinal Cord Hook. The minimally traumatic elastic cuff electrodes (Micro Cuff Sling, 200  $\mu\text{m}$ /3pol/2,5mm/cable entry top, CorTec GmbH) were gently placed under the nerve. The cuff electrode cable ends were soldered to a Male Miniature Pin Connector (520200, A-M Systems) and attached to the female connector, which had been soldered to a recording headstage. The surgery area was protected with mineral oil. Laser pulses were delivered directly to the nerve trunk by an Opto Probe Tips (Doric Lenses) connected to an Opto Probe Holder (Doric), and guided by a Micropositioner (P-10, Wafer Probe). Laser pulses timestamps were synchronized to the recordings via external TTL pulses into the TDT system.

**In vivo Electrophysiological recordings**—Mice were placed on the stereotaxic apparatus and one electrode array consisting of 16 tungsten microwires (35- $\mu\text{m}$  diameter, OMN1005, TDT systems) was implanted onto dorsal striatum (AP:+1.5 ML:1.5 DV:-2.5). Locations of electrodes were confirmed histologically. Recordings were performed using a multichannel acquisition processor (Tucker-Davis Technologies) concomitantly to optogenetic stimulation of nodose ganglion with blue light or green light. The multichannel processor recorded the laser pulses timestamps and neuronal activities simultaneously. Only single neurons with action potentials of signal-to-noise ratios >3:1 were analyzed. The action potentials were isolated online using voltage-time threshold windows and a three-principal component contour templates algorithm. Spikes were resorted using the Offline Sorter software (Plexon, Inc.).

**Slice electrophysiology**—The coronal slices containing the parabrachial area (PBN) were prepared from C57B6 mice. Briefly, mice were anesthetized with isoflurane and then decapitated. Then brains were rapidly removed and immersed in cold (4°C) and oxygenated high-sucrose solution containing (mM): sucrose 220, KCl 2.5,  $\text{NaH}_2\text{PO}_4$  1.23,  $\text{NaHCO}_3$  26,  $\text{CaCl}_2$  1,  $\text{MgCl}_2$  6 and glucose 10, pH 7.3 with NaOH). After being trimmed to a small tissue block containing the PBN, coronal slices (300  $\mu\text{m}$  thick) were cut on a vibratome and maintained at room temperature (23–25 °C) in a holding chamber with artificial cerebrospinal fluid (ACSF) (bubbled with 5%  $\text{CO}_2$  and 95%  $\text{O}_2$ ) containing (in mM): NaCl 124, KCl 3,  $\text{CaCl}_2$  2,  $\text{MgCl}_2$  2,  $\text{NaH}_2\text{PO}_4$  1.23,  $\text{NaHCO}_3$  26, glucose 10, pH 7.4 with NaOH for recovery and storage. After recovery at room temperature for at least one hour, slices were transferred to a recording chamber constantly perfused with ACSF at a temperature of 33 °C and a perfusion rate of 2 ml/min for electrophysiological experiments. Whole-cell patch clamp recording was performed in YFP-positive neurons in the parabrachial area under both voltage and current clamp. Micropipettes (3–4 M $\Omega$ ) were made of borosilicate glass (World Precision Instruments) with a Sutter P-97 micropipette puller and back filled with a pipette solution containing (mM): K-gluconate 135,  $\text{MgCl}_2$  2, HEPES 10, EGTA 1.1, Mg-ATP 2.5,  $\text{Na}_2$ -GTP 0.3, and  $\text{Na}_2$ -phosphocreatin 10, pH 7.3 with KOH. Both input resistance and series resistance were monitored throughout the experiments and the former

was partially compensated. Only recordings with stable series resistance and input resistance were accepted. To stimulate neurons with an optogenetic method, an LED-generated blue light pulses at different frequencies (5, 10 and 20 Hz) were applied to recorded neurons. All data were sampled at 3–10 kHz, filtered at 3 kHz and analyzed with an Apple Macintosh computer using Axograph X (AxoGraph).

## Behavioral Studies

**Behavioral apparatus for flavor conditioning and dry lick tests:** Behavioral experiments were conducted in either one of three identical mouse behavior chambers enclosed in a ventilated and sound-attenuating cubicle (Med Associates Inc., St. Albans, VT). Each chamber is equipped with two slots for sipper tubing placements, at symmetrical locations on one of the cage walls. All sippers are connected to a contact-based licking detection device allowing for measurements of licking responses with 10ms resolution. All lick timestamps were saved in a computer file for posterior analysis. Software controlled lasers and infusion pumps equipped with TTL input devices were connected to the behavioral chambers and programmed to automatically trigger laser or intra-gastric infusions in response to the detection of licks. MED-PC IV (Med Associates) was used as the platform for programming all experiments.

**Stimuli:** Nutritive intra-gastric stimuli were fat emulsions (IntraLipid®, Baxter Healthcare, Deerfield, IL). The stock emulsion contains as main components 30% soybean oil, 1.2% egg yolk phospholipids, 1.7% glycerin, and water. The caloric density of 30% IntraLipid® is 3.0 Kcal/mL, with 2.7 Kcal/mL accounted for by soybean oil and 0.3 Kcal/mL by phospholipids + glycerin. The original 30% emulsion was diluted into an emulsifying control solution (1.2% phospholipids + 1.7% glycerine, in water) in order to prepare the 5% and 20% dilutions. Intra-gastric LiCl was prepared at 2.5mM/Kg, prepared in physiological saline, which was used as control stimulus.

**Flavor-nutrient conditioning:** For rewarding conditioning tests, mice were trained to produce licks to spouts containing non-caloric flavored solutions in order to receive one intra-gastric infusion of either 20% IntraLipid or 5% IntraLipid depending on the identity of the flavor being ingested. The choice of concentrations was based on previous studies demonstrating their effects during reward tests. For avoidance conditioning tests, protocols were identical except that intra-gastric infusions of 2.5mM/Kg LiCl were paired to one of the flavors, and saline to the remaining flavor. In all cases, the exterior part of the gastric catheter was connected to a segment of MicroRenathane tubing secured to the tip of a 3mL standard syringe containing the solutions to be infused and mounted on the syringe pump. The syringe pump was placed near a small hole made on the superior part of the sound attenuating box in such a way that mice could move freely inside the behavioral chambers. During the task, the detection of the first 200 licks triggered an intra-gastric infusion of the solution; the slow infusions lasted for 20 min at a rate of 30 $\mu$ L/min (total volume: 0.6mL). Licks detected during and after the infusions had no programmed consequences (i.e. did not result in additional infusions). This experimental design was chosen to eliminate possible confounds related to differences in intake. For IntraLipid tests, “conditioning sessions” lasted for 1 hour and were performed for 6 consecutive days under food (16h) deprivation,

alternating daily the flavor-lipid association. Thus, there were 3 sessions associated with each specific Flavor-lipid pair. For LiCl tests, “conditioning sessions” also lasted for 1 hour but were performed for only 2 consecutive days and the rate of the infusion was adjusted to match the corresponding LiCl dose. Importantly, for each animal, flavors were arbitrarily paired with either infusate, thereby preventing flavor identity to influence preference formation. Short-term (5 min) two-bottle preference tests between the two distinct flavors were performed previous to and following the conditioning sessions. These tests were performed in extinction, *i.e.* in the absence of intra-gastric infusions. Short-duration of this test aims to minimize postingestive influences. After conditioning, an identical test was performed to assess the formation of flavor preferences. The number of licks for each Flavor was recorded and used to calculate the preference ratio as follows:

$$\text{Preference ratio for Flavor1} = \frac{n(\text{Flavor1})}{n(\text{Flavor1}) + n(\text{Flavor2})}$$

where  $n(\text{Flavor}x)$  denotes the detected number of licks to Flavor  $x$  during a given session. To eliminate the influence of side-biases mice were tested four consecutive times with sipper positions being switched between any two consecutive tests, with the overall average across trials defined as the actual preference. Flavor conditioning sessions where optical stimulation was used as the unconditioned stimulus were performed identically as above, except that in this case licks triggered 9sec-long blue light pulses (473-nm) via TTL pulses, coupling consumption to laser activation. Licks detected while the laser was on had no programmed consequences.

**Dry lick-triggered intra-gastric feeding:** Mice were trained to produce licks to a dry metallic spout in order to receive intra-gastric infusions of the fat emulsions. The exterior part of the gastric catheter was connected to a segment of MicroRenathane tubing secured to the tip of a 3 mL standard syringe containing the solutions to be infused and mounted on the syringe pump. The syringe pump was placed near a small hole made on the superior part of the sound attenuating box in such a way that mice could move freely inside the behavioral chambers. During the task, a detected dry lick triggered an intra-gastric infusion of the fat emulsion that lasted for 6 seconds at a rate of 0.6 mL/min. However, licks detected while an infusion was taking place had no programmed consequences (*i.e.* did not result in additional infusions). Experimental tests lasted for 1 hour. Animals were tested once a day in their responses to one single concentration of IntraLipid (20%). In order to train the animals in this task, once mice had recovered from surgery and been habituated to the behavioral chambers, a small amount of standard chow was placed behind the spout’s orifice (so that they could be smelled but not reached) to prime naive animals to dry lick and obtain intra-gastric infusions. Training sessions lasted for 1 h and were performed daily under food (20 h) deprivation. After 4 priming sessions, clean odorless spouts replaced the ones containing chow. Animals were considered trained to perform the experiments once they showed less than 10% between-session variability, a criterion reached within 10 consecutive sessions.

**Online place preference and avoidance tests (optogenetics):** Place preference tests made use of automated video analyses (EthoVision XT11.5, Noldus). A rat behavioral cage was prepared in such a way that the floor of one half of the cage was covered by bedding

(preferred by all mice) and the floor of the other half of the cage was covered by an acrylic platform (less preferred by all mice). To demonstrate place preferences, the less preferred area of the test cage was associated with switching the laser source ON, in such a way that the presence of the mouse in this area of the cage switched the laser source ON via a TTL board under control of the camera monitoring. To demonstrate place avoidance, the preferred area of the test cage was associated with switching the laser source ON. Quantification of occupancy of different areas of the cage made use of automated video analyses (EthoVision XT11.5, Noldus).

**Acquired place preference (chemogenetics):** A rat behavioral cage was prepared in such a way that the floor of one half of the cage was covered by bedding (preferred by all mice), whereas the floor of the other half of the cage was covered by an acrylic platform (less preferred by all mice). During conditioning, transit between the two halves was blocked. In alternate daily sessions, the less preferred area of the test cage was associated with CNO injections and the preferred area of the test cage associated with vehicle control injections. Before placing the animals in the corresponding half, the exterior part of the gastric catheter was connected to a segment of MicroRenathane tubing secured to the tip of a 3mL standard syringe containing the solutions to be infused and mounted on the syringe pump. During **all** sessions, mice were administered with an intra-gastric infusion of 0.3kCal IntraLipid (rate: 30  $\mu$ L/min; total volume: 0.6mL of 5% IntraLipid). Both previous to and after the 6 1h-daily conditioning sessions, a 10min preference test was performed in such a way that the animal was free to transit between the two halves of the test cage. Quantification of occupancy of different areas of the cage made use of automated video analyses (EthoVision XT11.5, Noldus).

**Nose poke task (self-stimulation behavior):** Mice were placed in an operant box equipped with two slots for nose poke slots at symmetrical locations on one of the cage walls. Nose poke slots were connected to a photo-beam detection device allowing for measurements of responses with 10-ms resolution, and only one of them triggered the 1s-long laser pulses. The active side was counterbalanced among animals, and responses detected while the laser was on had no programmed consequences. Three consecutive days of 30 min stimulation sessions were performed, and on the fourth day one 30min-long extinction test was performed (*i.e.* both nose poke detectors were inactive). Timestamps associated with all behavioral and laser events were saved in a computer file for posterior analysis.

**Optical Stimulation regimens:** Stimulation frequencies were chosen according to the outcome of the nerve or slice electrophysiological studies. Although we did not detect major differences between stimulation frequencies in terms of evoking (or failing to) behavior, we used the 1Hz frequencies for nodose ganglia terminals stimulation, and for either VGlut2-positive or VGat-positive parabrachial neurons and/or terminals, a 10Hz frequency was chosen. Intensity at tip of fibers was estimated at approximately 5 mW.

**Chemogenetic activation:** Clozapine-N-Oxide (1mg/kg, Enzo Life Sciences) or Clozapine (0.1mg/kg, Sigma) was injected *i.p.*, 10mins before the start of the behavioral sessions.

**Food intake and Fos induction upon CCK and LiCl injections**—Mice were single caged and 2.5g chow/day food restricted and divided into three groups: Saline-injected, CCK-injected and LiCl-injected. The CCK (10 g/kg, AnaSpec Inc. Fremont, CA) and LiCl (2.5mg/kg) doses were chosen for producing a statistically identical 50% reduction in food intake. Fifteen minutes after the injections animals were allowed *ad libitum* access to chow and after 1hour free consumption, the pellets were removed and weighted. For *Fos* studies, mice were also single caged and 2.5g chow/day food restricted and divided into three groups: Saline-injected, CCK-injected and LiCl-injected. The same CCK and LiCl doses chosen for producing a statistically identical 50% reduction in food intake were used (CCK 10 g/kg, LiCl 2.5mg/kg), although for *Fos* measurements no food intake was allowed after the injections. Animals were perfused 90 minutes after the administration of the injections.

**Oxygen consumption, respiration and heart rate measurements:** Both breathing and heart rates were measured by pulse oximetry using the MouseOx Plus (Starr Life Sciences Corp, USA) in accordance with manufacturer's instructions. Briefly, each mouse was mildly anaesthetized using 5% isoflurane and shaved in the neck to place a Collar Clip Sensor. Measurements were performed under mild anesthesia to collect representative, error-free data due to the motion artifacts.

Oxygen consumption was measured via indirect calorimetry using the Oxymax/CLAMS Animal Monitoring System (Columbus Instruments, Columbus, OH), a mouse-dedicated, 4-cage system equipped with open-circuit calorimetry. Metabolism-induced heat was derived by assessing the exchange of oxygen for carbon dioxide that occurs during metabolic processes, as measured by the mass flow principle. Oxygen (O<sub>2</sub>) measurement was performed via paramagnetic sensing and carbon dioxide (CO<sub>2</sub>) by single beam non-dispersed IR. The respective volumes were determined as:

$$VO_2 = V_i O_{2i} - V_o O_{2o} \quad (1)$$

$$VCO_2 = V_o CO_{2o} - V_i CO_{2i} \quad (2)$$

where: V<sub>i</sub> = Mass of air at chamber input per unit time, V<sub>o</sub> = Mass of air at chamber output per unit time, O<sub>2i</sub> = Oxygen fraction in V<sub>i</sub>, CO<sub>2i</sub> = Oxygen fraction in V<sub>i</sub>, O<sub>2o</sub> = Carbon Dioxide fraction in V<sub>o</sub>, CO<sub>2o</sub> = Carbon Dioxide fraction in V<sub>o</sub>.

### Quantification and Statistical Analyses

Data analyses, excluding all electromyogram/electrophysiological data, were performed using SPSS (v.21.0, IBM Predictive Software), Ethovision XT 11.5 (Noldus), GraphPad Prism 7 (GraphPad) and Matlab (v.17b, MathWorks), Spike2 (Cambridge Electronic Design Ltd). Animals assigned to the different experimental groups were experimentally naïve littermates, so that no randomization or other a priori criteria were adopted for group assignments. Experimental manipulations were analysed according to within-subject

repeated-measures designs. Order of experimental conditions was randomly assigned across subjects. Samples sizes were chosen based on our previous studies employing similar optogenetic, electrophysiological and neuronal ablation approaches. Samples sizes adopted in our current study were sufficient for detecting strong effect sizes while complying with guidelines from local enforcing rules requesting minimal animal usage by J.B. Pierce's Institutional Animal Care and Use Committee. Experimenters were not blind to experimental conditions. Only animals carrying signs of distress/infection/bleeding/anorexia after the surgical procedures were excluded. Data from all animals used in the experiments were included in the final analyses and plots.

**Analysis of Behavioral trials**—For all behavioral studies, including those resulting from pathway-targeted lesions, optogenetics and/or chemogenetic experiments, analyses made use of standard linear models (Pearson correlation), as well as one- or two-way (repeated measures) ANOVAs and post-hoc t-tests whenever relevant, for correcting for multiple comparisons. All data were reported as mean±SEM. In all cases sample sizes (N) denote number of animals used. All p-values associated with the t-tests performed correspond to two-tailed tests, and all post-hoc tests were corrected for multiple comparisons by employing Bonferroni correction. To assess potentially spurious results associated with non-normality, all significant effects were confirmed by rerunning the tests using the appropriate non-parametric test. All data are individually plotted (Prism 7, GraphPad), and the corresponding bar plot of the precision measures (mean ± SEM) were overlaid on the figure. The exact value of all N (always number of animals), df, T/F, and p values are reported in the figure legends. An effect was considered statistically significant whenever the corresponding statistic was associated with a p-value (Bonferroni-corrected when appropriate) strictly less than 0.05.

**Analysis of In-vivo electrophysiological data**—Data were then imported into Matlab (v.17b, MathWorks) for analysis using the custom-written software. Ninety-three single neurons displaying action potentials of signal-to-noise ratios >3:1, were analysed. Otherwise data were discarded. To calculate firing rates, instantaneous firing rates were smoothed using the Matlab filtering function with a 60 s moving average using 50 ms bins. To test for significance in firing rate changes, we used an individual unit analysis. A Kruskal-Wallis test ( $p < 0.05$ ) was performed on each unit to determine whether the mean firing rate during the optogenetic period of stimulation was significantly different from the baseline mean firing rate, and based on this criterium units were classified as modulated or not modulated. The baseline was taken from the start of session until the first optical stimulation pulse. For all neurons recorded, the PSTH were arranged in a matrix (neurons=rows and bins=columns). The rows of the matrix were normalized as z-scores and then plotted using the first component of the principal component analysis (PCA) (Matlab toolboxes and custom-written scripts) aligned to optogenetic blue light stimulation (start or end respectively). In all cases, the first component had a higher explained variance.

**Analysis of In-vivo nerve recordings and electromyogram data**—To perform the analyses, the signals were full-wave rectified and root mean square (RMS)-converted within moving windows of 25-ms duration. Baseline signals (obtained from those periods during

which the laser source was off) were used to establish a cut-off  $C_{off}$  value defined by the overall session mean  $M_s$  and associated standard deviation  $STD_s$  of the signals as

$$C_{off} = M_s + (3 \times STD_s)$$

This cut off value was then used to determine whether the signal ( $S$ ) at a given time point was significantly different from baseline (*i.e.*  $S > C_{off}$ ). Each time point in which this inequality holds true were defined as an “event”. These analyses were performed using custom software programmed in MATLAB (v.17b, MathWorks) and are available upon request.

## DATA AND SOFTWARE AVAILABILITY

Custom software is available. See Key Resources Table above for download details.

## KEY RESOURCES TABLE

REAGENT or RESOURCE	SOURCE	IDENTIFIER
Antibodies		
Goat Anti-GFP antibody (FITC)	Abcam	Cat# ab6662 RRID:AB_305635
Rabbit-anti-mCherry	Abcam	Cat# ab167453 RRID:AB_2571870
Alexa Fluor® 647 recombinant rabbit monoclonal anti-Neuronal Nuclei (NeuN)	Abcam	Cat# ab190565 RRID: EPR12763
Chicken polyclonal to Tyrosine Hydroxylase antibody	Abcam	Cat# ab76442 RRID: AB_1524535
Mouse anti-TH	ImmunoStar	Cat# 22941 RRID: AB_10731005
Goat polyclonal to CGRP	Abcam	Cat# ab36001 RRID:AB_725807
Alexa Fluor® 488 conjugated affininpure goat anti-chicken IgY (H&L)	Abcam	Cat# ab150169 RRID:AB_2636803
Anti-c-Fos Rabbit polyclonal to c-Fos	Abcam	Cat# ab 190289 RRID: AB_2231989
TRITC-conjugated affininpure Goat anti-Rabbit IgG (H+L)	Jackson ImmunoResearch Labs	Cat# 111-025-144 RRID:AB_2337932
FITC-conjugated affininpure goat anti-rabbit IgG (H+L)	Jackson ImmunoResearch Labs	Cat# 111-095-144 RRID:AB_2337978
FITC-conjugated affininpure Donkey Anti-Goat IgG (H+L)	Jackson ImmunoResearch Labs	Cat# 705-095-147 RRID:AB_2340401
TRITC-conjugated affininpure Donkey Anti-Goat IgG (H+L)	Jackson ImmunoResearch Labs	Cat# 705-025-147 RRID:AB_2340389
Biotinylated Goat Anti-Rabbit IgG antibody	Vector Laboratories	Cat# BA-1000 RRID:AB_2313606
Goat anti-Phaseolus Vulgaris Agglutinin (E+L), Unconjugated	Vector Laboratories	Cat# AS-2224 RRID: AB_10000080
Rabbit anti-PHA-L	Dako	Cat# B275 RRID: AB_2315137

REAGENT or RESOURCE	SOURCE	IDENTIFIER
Rabbit anti-FG	Chemicon®, Millipore	Cat# AB153-I RRID: AB_2632408
Chemicals, Peptides, and Recombinant Proteins		
FluoroGold (FG)	Manufacturer: Fluorochrome Inc; Purchased from Fisher scientific	Cat# NC0560981
PHA-L	Vector	Cat# L-1110
Red RetroBeads	Lumafluor	N/A
CCK-SAP	Advanced Targeting Systems	Cat # IT-31
SAP	Advanced Targeting Systems	Cat # IT-21
CCK8	AnaSpec	Cat # AS-20739
Clozapine N-oxide (CNO)	Enzo Life Sciences	Cat # BML-NS105-0025
Clozapine	Sigma	Cat # C6305-25MG
cis-(Z)-Flupenthixol dihydrochloride	Sigma	Cat # F114
Metrocloramide Hydrochloride	Sigma	Cat # M0763-10G
Critical Commercial Assays		
VECTASTAIN Elite ABC HRP Kit (Peroxidase, Standard)	Vector Laboratories	Cat# PK-6100
Experimental Models: Organisms/Strains		
Mouse: C57BL/6J	The Jackson Laboratory	JAX: 000664
Mouse: Slc32a1 <sup>tm2(cre)Low1/J</sup>	The Jackson Laboratory	JAX: 016962
Mouse: Slc17a6 <sup>tm2(cre)Low1/J</sup>	The Jackson Laboratory	JAX: 016963
Mouse: Slc6a3 <sup>tm1.1(cre)Bkmm/J</sup>	The Jackson Laboratory	JAX: 006660
Mouse: Agrp <sup>tm1(cre)Low</sup>	The Jackson Laboratory	JAX: 012899
Mouse: B6;129S-Gt(ROSA)26Sor <sup>tm34.1(CAG-Syp/td Tomato)Hze/J</sup>	The Jackson Laboratory	JAX: 012570
B6.Cg-Gt(ROSA)26Sor <sup>tm14(CAG-tdTomato)Hze/J</sup>	The Jackson Laboratory	JAX: 007914
Recombinant DNA		
AAVrg-pmSyn1-EBFP-Cre	Dr. Zeng-Addgene AAV Viral Service	51507
H129	NIH Center for Neuroanatomy with Neurotropic Virus	TK-TT
SAD- G-GFP	Dr. Diego V. Bohórquez, Assistant Professor Duke Medicine-GI and Neurobiology	N/A
AAV5-EF1a-DIO-hChR2(H134R)-EYFP	Dr. Karl Deisseroth-University of North Carolina's Vector Core	N/A
AAV5-EF1a-DIO-EYFP	Dr. Karl Deisseroth-University of North Carolina's Vector Core	N/A
AAV-hSyn-DIO-rM3D(Gs)-mCherry	Dr. Bryan Roth - University of North Carolina's Vector Core	N/A
AAV5-flex-taCasp3-TEVp	Dr. Nirao Shah - University of North Carolina's Vector Core	N/A
AAV5-CA-FLEX-RG	Dr. Naoshige - UchidaUniversity of North Carolina's Vector Core	N/A

REAGENT or RESOURCE	SOURCE	IDENTIFIER
AAV8.2-hEF1a-DIO-synaptophysin-EYFP	Viral Gene Transfer Core, McGovern Institute for Brain Research, Massachusetts Institute of Technology	N/A
CAV2-Cre-GFP	Institut de Génétique Moléculaire de Montpellier, France (Junyent and Kremer, 2015)	N/A
PRV-GFP	NIH Center for Neuroanatomy with Neurotropic Virus	152
PRV-RFP	NIH Center for Neuroanatomy with Neurotropic Virus	614
Software and Algorithms		
Matlab R20 17b	MathWorks	<a href="http://www.mathworks.com/products/matlab/">http://www.mathworks.com/products/matlab/</a>
Offline Sorter	Plexon	<a href="http://www.plexon.com/products/offline-sorter">www.plexon.com/products/offline-sorter</a>
PatchMaster 2.20	HEKA	<a href="http://www.heka.com/index.html">http://www.heka.com/index.html</a>
Igor Pro 6.36	WaveMetrics	<a href="https://www.wavemetrics.com/">https://www.wavemetrics.com/</a>
EthoVision XT 11.5	Noldus	<a href="http://www.noldus.com/animal-behaviorresearch/pro">http://www.noldus.com/animal-behaviorresearch/pro</a>
LabView 2014	LabView	<a href="http://www.ni.com/download/labviewdevelopment-s">http://www.ni.com/download/labviewdevelopment-s</a>
GraphPad Prism 7	GraphPad	<a href="http://www.graphpad.com/scientificsoftware/prism/">http://www.graphpad.com/scientificsoftware/prism/</a>
Adobe design standard CS6	Adobe	<a href="http://shop.adobe.com/store/adbehme/en_IE/pd/Ther">http://shop.adobe.com/store/adbehme/en_IE/pd/Ther</a>
SPSS 21.0	IBM Predictive Software	<a href="https://www.ibm.com/support/knowledgecenter/SSL">https://www.ibm.com/support/knowledgecenter/SSL</a>
Spike2 version 7	CED (Cambridge Electronic Design Ltd)	<a href="http://ced.co.uk/products/spkovin">http://ced.co.uk/products/spkovin</a>
ImageJ bundled with 64-bit Java 1.8.0_112	NIH ImageJ	<a href="https://imagej.nih.gov/ij/index.html">https://imagej.nih.gov/ij/index.html</a>
Other		
IntraLipid 20%, emulsion	Sigma	I141-100ML
Totally Light 2Go - non-caloric powdered flavor drink mix, cranberry and wild berry flavors; sugar-free, Splenda-sweetened	4C Foods Corp.	N/A
Implantable Optical Fibers	Doric Lenses, Canada	MFC_200/240-0.22_6mm_ZF1.25(G)_FLT
Formvar-Insulated Nichrome Wires (EMG recording)	A-M system	Cat # 762000
Male Miniature Pin Connector Fits Model 1800 / 3000 Headstage Leads (EMG recording)	A-M system	Cat # 520200
Female Miniature Pin Connector Fits A-M Systems' electrodes (EMG recording)	A-M system	Cat # 520100
A-M Systems 1700 AC Amplifier	A-M systems	Cat # 690000
2mm, cut off 6kDa, Microdialysis Probe and guide cannula	CMA	CMA-7,
16 tungsten microwires, 35- $\mu$ m diameter (Electrophysiological recordings)	TDT systems	Cat # OMN1005
The minimally traumatic elastic cuff electrodes (Micro Cuff Sling (200 $\mu$ m/3pol/2,5mm/ cable entry top)	CorTec GmbH	N/A
Infra-red pulse oximeter	Starr Life Sciences Corp	MouseOx Plus
Collar Clip Sensor	MouseOx Plus Sensor, Starr Life Sciences Corp	SLS-015 021
MATLAB script for electromyogram detection	de Araujo lab	<a href="https://www.dropbox.com/sh/6b3y7ult47m8mje/AA">https://www.dropbox.com/sh/6b3y7ult47m8mje/AA</a>
MATLAB script for PCA calculation of neuronal data	de Araujo lab	<a href="https://www.dropbox.com/sh/ei2o6hdcqp4t8zf/AAB">https://www.dropbox.com/sh/ei2o6hdcqp4t8zf/AAB</a>

REAGENT or RESOURCE	SOURCE	IDENTIFIER
Spike2 scripts to count neurogram and myogram events	de Araujo lab	<a href="https://github.com/matthewperkins/WH_IdA_Vagus">https://github.com/matthewperkins/WH_IdA_Vagus</a>

## Supplementary Material

Refer to Web version on PubMed Central for supplementary material.

## Acknowledgments

Supported by US National Institutes of Health grants R01CA180030, R01DC014859 (I.E.d.A.); R00DK094871 (G.d.L.). We thank M. McDougle for assistance with behavioral assays, M. Klein, K. Buchannan for packaging the rabies constructs, vagal recordings, and members of R. Medzhitov lab (Yale) for assisting breathing, heart rate measurements.

## References

- Altschuler SM, Bao XM, Bieger D, Hopkins DA, and Miselis RR (1989). Viscerotopic representation of the upper alimentary tract in the rat: sensory ganglia and nuclei of the solitary and spinal trigeminal tracts. *J Comp Neur* 283, 248–268. [PubMed: 2738198]
- Angyan L (1975). Vagal influences on hypothalamic self-stimulation in the cat. *Life Sci* 17, 289–292. [PubMed: 1099379]
- Banfield BW, Kaufman JD, Randall JA, and Pickard GE (2003). Development of pseudorabies virus strains expressing red fluorescent proteins: new tools for multisynaptic labeling applications. *J Virol* 77, 10106–10112. [PubMed: 12941921]
- Berthoud HR (2008). Vagal and hormonal gut-brain communication: from satiation to satisfaction. *Neurogastroenterol Motil* 20 Suppl 1, 64–72. [PubMed: 18402643]
- Betley JN, Xu S, Cao ZFH, Gong R, Magnus CJ, Yu Y, and Sternson SM (2015). Neurons for hunger and thirst transmit a negative-valence teaching signal. *Nature* 521, 180–185. [PubMed: 25915020]
- Beutler LR, Chen Y, Ahn JS, Lin YC, Essner RA, and Knight ZA (2017). Dynamics of Gut-Brain Communication Underlying Hunger. *Neuron* 96, 461–475 e465. [PubMed: 29024666]
- Bohorquez DV, and Liddle RA (2015). The gut connectome: making sense of what you eat. *J Clin Invest* 125, 888–890. [PubMed: 25729849]
- Campos CA, Bowen AJ, Schwartz MW, and Palmiter RD (2016). Parabrachial CGRP Neurons Control Meal Termination. *Cell Metab* 23, 811–820. [PubMed: 27166945]
- Carreno FR, and Frazer A (2017). Vagal Nerve Stimulation for Treatment-Resistant Depression. *Neurotherapeutics* 14, 716–727. [PubMed: 28585221]
- Carter ME, Soden ME, Zweifel LS, and Palmiter RD (2013). Genetic identification of a neural circuit that suppresses appetite. *Nature* 503, 111–114. [PubMed: 24121436]
- Chang RB, Strohlic DE, Williams EK, Umans BD, and Liberles SD (2015). Vagal Sensory Neuron Subtypes that Differentially Control Breathing. *Cell* 161, 622–633. [PubMed: 25892222]
- Clemmensen C, Muller TD, Woods SC, Berthoud HR, Seeley RJ, and Tschop MH (2017). Gut-Brain Cross-Talk in Metabolic Control. *Cell* 168, 758–774. [PubMed: 28235194]
- Coizet V, Dommert EJ, Klop EM, Redgrave P, and Overton PG (2010). The parabrachial nucleus is a critical link in the transmission of short latency nociceptive information to midbrain dopaminergic neurons. *Neuroscience* 168, 263–272. [PubMed: 20363297]
- Corbett EK, Sinfield JK, McWilliam PN, Deuchars J, and Batten TF (2005). Differential expression of vesicular glutamate transporters by vagal afferent terminals in rat nucleus of the solitary tract: projections from the heart preferentially express vesicular glutamate transporter 1. *Neuroscience* 135, 133–145. [PubMed: 16084661]
- Crow TJ (1971). The relation between electrical self-stimulation sites and catecholamine-containing neurons in the rat mesencephalon. *Experientia* 27, 662. [PubMed: 5556448]

- Crow TJ (1973). Catecholamine-containing neurones and electrical self-stimulation. 2. A theoretical interpretation and some psychiatric implications. *Psychol Med* 3, 66–73. [PubMed: 4692492]
- de Araujo IE, Tellez LA, Ferreira JG, Ren X, and Yeckel CW (2012). The gut-brain dopamine axis: A regulatory system of caloric intake. *Physiol & Behav* 106, 394–399. [PubMed: 22406348]
- de Lartigue G, and Diepenbroek C (2016). Novel developments in vagal afferent nutrient sensing and its role in energy homeostasis. *Curr Opin Pharmacol* 31, 38–43. [PubMed: 27591963]
- Diepenbroek C, Quinn D, Stephens R, Zollinger B, Anderson S, Pan A, and de Lartigue G (2017). Validation and characterization of a novel method for selective vagal deafferentation of the gut. *Am J Physiol* 313, G342–G352.
- Farrell MS, Pei Y, Wan Y, Yadav PN, Daigle TL, Urban DJ, Lee HM, Sciaky N, Simmons A, Nonneman RJ, et al. (2013). A Galphas DREADD mouse for selective modulation of cAMP production in striatopallidal neurons. *Neuropsychopharmacology* 38, 854–862. [PubMed: 23303063]
- Howland RH (2014). Vagus Nerve Stimulation. *Curr Behav Neurosci Rep* 1, 64–73. [PubMed: 24834378]
- Hull CL (1943). *Principles Of Behavior: An Introduction to Behavior Theory* (New York: Appleton-Century-Crofts).
- Ingram S, and Williams JT (1994). Opioid Inhibition of I<sub>h</sub> via Adenylyl Cyclase. *Neuron* 13, 179–186. [PubMed: 7519024]
- Junyent F, and Kremer EJ (2015). CAV-2--why a canine virus is a neurobiologist's best friend. *Curr Opin Pharmacol* 24, 86–93. [PubMed: 26298516]
- Kaur S, Pedersen NP, Yokota S, Hur EE, Fuller PM, Lazarus M, Chamberlin NL, and Saper CB (2013). Glutamatergic signaling from the parabrachial nucleus plays a critical role in hypercapnic arousal. *J Neurosci* 33, 7627–7640. [PubMed: 23637157]
- Lo L, and Anderson DJ (2011). A Cre-dependent, anterograde transsynaptic viral tracer for mapping output pathways of genetically marked neurons. *Neuron* 72, 938–950. [PubMed: 22196330]
- Madisen L, Mao T, Koch H, Zhuo JM, Berenyi A, Fujisawa S, Hsu YW, Garcia AJ, 3rd, Gu X, Zanella S, et al. (2012). A toolbox of Cre-dependent optogenetic transgenic mice for light-induced activation and silencing. *Nat Neurosci* 15, 793–802. [PubMed: 22446880]
- Mayer EA (2011). Gut feelings: the emerging biology of gut-brain communication. *Nat Rev Neurosci* 12, 453–466. [PubMed: 21750565]
- McGovern AE, Davis-Poynter N, Yang SK, Simmons DG, Farrell MJ, and Mazzone SB (2015). Evidence for multiple sensory circuits in the brain arising from the respiratory system: an anterograde viral tract tracing study in rodents. *Brain Struct Funct* 220, 3683–3699. [PubMed: 25158901]
- Norgren R, and Smith GP (1988). Central distribution of subdiaphragmatic vagal branches in the rat. *J Comp Neur* 273, 207–223. [PubMed: 3417902]
- Olds J (1976). Do Reward and Drive Neurons Exist? In *Psychopathology of Human Adaptation* Serban G, ed. (Boston, MA: Springer).
- Olds J, and Milner P (1954). Positive reinforcement produced by electrical stimulation of septal area and other regions of rat brain. *J Comp Physiol Psychol* 47, 419–427. [PubMed: 13233369]
- Palmiter RD (2008). Dopamine signaling in the dorsal striatum is essential for motivated behaviors: lessons from dopamine-deficient mice. *Ann NY Acad Sci* 1129, 35–46. [PubMed: 18591467]
- Perez C, and Sclafani A (1991). Cholecystokinin conditions flavor preferences in rats. *Am J Physiol* 260, R179–185. [PubMed: 1992819]
- Phillips AG, Carter DA, and Fibiger HC (1976). Dopaminergic substrates of intracranial self-stimulation in the caudate-putamen. *Brain Res* 104, 221–232. [PubMed: 1260420]
- Prechtl JC, and Powley TL (1990). The fiber composition of the abdominal vagus of the rat. *Anat Embryol* 181, 101. [PubMed: 2327594]
- Puizillout J-J (2005). *Central projections of vagal afferents*. (Paris: Éditions Publibook).
- Schultz W (2015). Neuronal Reward and Decision Signals: From Theories to Data. *Physiol Rev* 95, 853–951. [PubMed: 26109341]

- Schwartz GJ (2000). The role of gastrointestinal vagal afferents in the control of food intake: current prospects. *Nutrition* 16, 866–873. [PubMed: 11054591]
- Scalafani A (2013). Gut-brain nutrient signaling. Appetition vs. satiation. *Appetite* 71, 454–458. [PubMed: 22664300]
- Shapiro RE, and Miselis RR (1985). The central organization of the vagus nerve innervating the stomach of the rat. *J Comp Neur* 238, 473–488. [PubMed: 3840183]
- Sharon G, Sampson TR, Geschwind DH, and Mazmanian SK (2016). The Central Nervous System and the Gut Microbiome. *Cell* 167, 915–932. [PubMed: 27814521]
- Smith GP, Jerome C, and Norgren R (1985). Afferent axons in abdominal vagus mediate satiety effect of cholecystokinin in rats. *Am J Physiol* 249, R638–641. [PubMed: 4061684]
- Sternson SM, and Roth BL (2014). Chemogenetic tools to interrogate brain functions. *Ann Rev Neurosci* 37, 387–407. [PubMed: 25002280]
- Su Z, Alhadeff AL, and Betley JN (2017). Nutritive, Post-ingestive Signals Are the Primary Regulators of AgRP Neuron Activity. *Cell Rep* 21, 2724–2736. [PubMed: 29212021]
- Tellez LA, Ferreira JG, Medina S, Land BB, DiLeone RJ, and de Araujo IE (2013). Flavor-independent maintenance, extinction, and reinstatement of fat self-administration in mice. *Biol Psychiatry* 73, 851–859. [PubMed: 23587200]
- Tervo DG, Hwang BY, Viswanathan S, Gaj T, Lavzin M, Ritola KD, Lindo S, Michael S, Kuleshova E, Ojala D, et al. (2016). A Designer AAV Variant Permits Efficient Retrograde Access to Projection Neurons. *Neuron* 92, 372–382. [PubMed: 27720486]
- Ungerstedt U (1971). Adipsia and aphagia after 6-hydroxydopamine induced degeneration of the nigrostriatal dopamine system. *Acta Physiol Scand Suppl* 367, 95–122. [PubMed: 4332694]
- Wickersham IR, Finke S, Conzelmann KK, and Callaway EM (2007). Retrograde neuronal tracing with a deletion-mutant rabies virus. *Nat Methods* 4, 47–49. [PubMed: 17179932]
- Williams EK, Chang RB, Strohlic DE, Umans BD, Lowell BB, and Liberles SD (2016). Sensory Neurons that Detect Stretch and Nutrients in the Digestive System. *Cell* 166, 209–221. [PubMed: 27238020]
- Wu Q, Clark MS, and Palmiter RD (2012). Deciphering a neuronal circuit that mediates appetite. *Nature* 483, 594–597. [PubMed: 22419158]
- Yang CF, Chiang MC, Gray DC, Prabhakaran M, Alvarado M, Juntti SA, Unger EK, Wells JA, and Shah NM (2013). Sexually dimorphic neurons in the ventromedial hypothalamus govern mating in both sexes and aggression in males. *Cell* 153, 896–909. [PubMed: 23663785]

**Highlights**

- Critical role for the vagal gut-to-brain axis in motivation and reward.
- Optogenetic stimulation of the vagal gut-to-brain axis produces reward behaviors.
- Asymmetric brain pathways of vagal origin mediate motivation and dopamine activity.
- Gut-innervating vagal sensory neurons are major components of the reward circuitry.

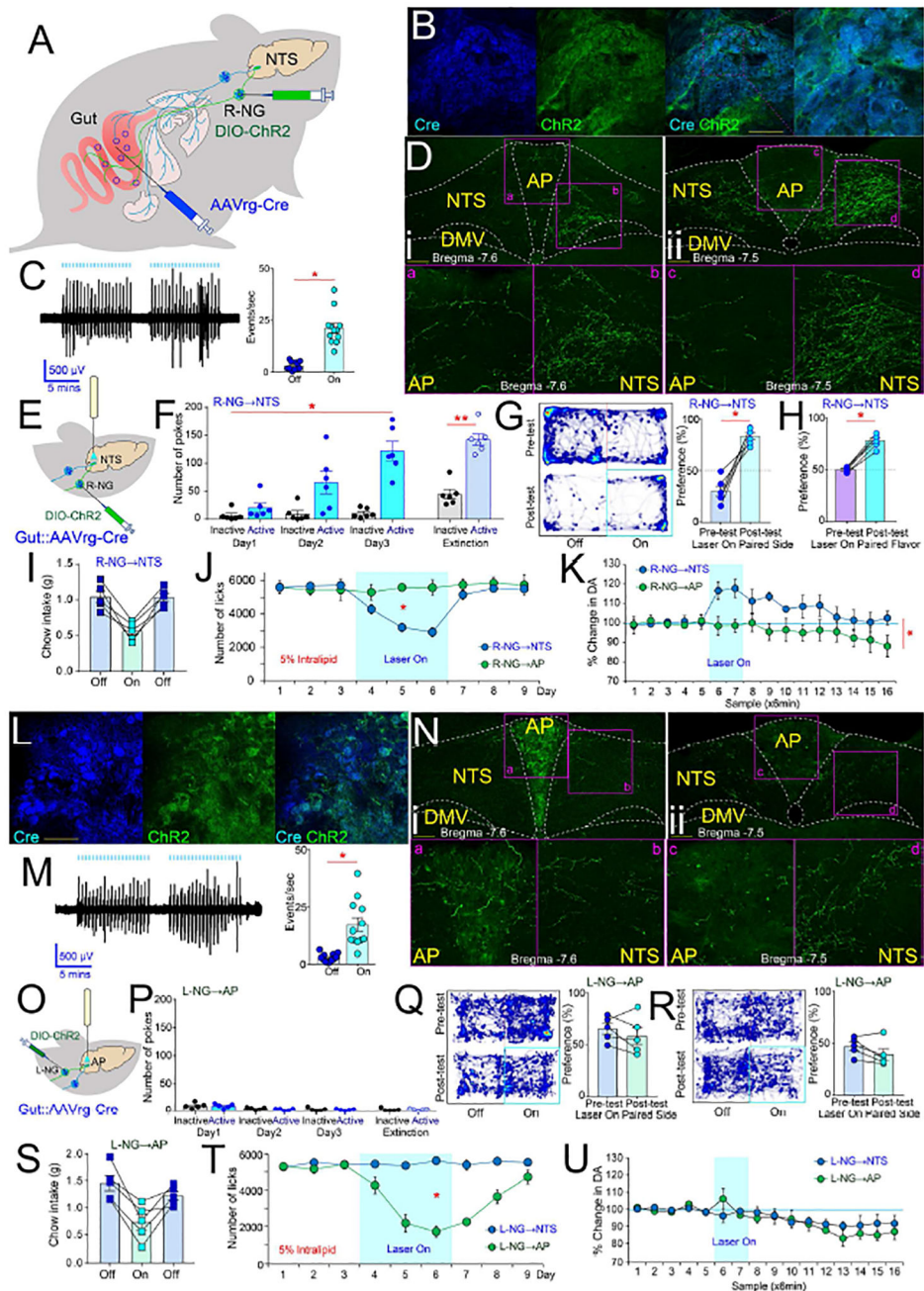


**Figure 1. Gut-brain optogenetics**

**A.** Combinatorial viral strategy to target gut vagal sensory neurons. **B.** *Cre*-EBFP and DIO-ChR2-EYFP detected in R-NG. Bar=100µM. **C.** *Left panel*: Vagal nerve fiber activity upon light stimulation of R-NG DIO-ChR2-EYFP-positive neurons. Trace shows responses locked to light pulses (blue bars on top). *Right panel*: Supra-threshold events during nerve recordings. N=12; paired t-test  $t[11]=8.7$  \* $p<0.001$ . **D.** R-NG DIO-ChR2-EYFP-positive terminals innervate ventromedial NTS at both anterior (*i*) and caudal (*ii*) levels (10×). Lower panels show delimited areas at 40×. AP (*a* and *c*) innervation was weaker than NTS (*b* and *d*) at both anterior (*i*) and caudal (*ii*) levels. Bar=100µM. **E.** Optical fibers above R-NG

terminals in NTS. **F.** RNG→NTS optical stimulation sustains self-stimulation. N=6; Two-way RM-ANOVA, Main effect of poking on the laser-paired hole *vs.* inactive hole  $F[1,5]=60.4$ ,  $p=0.001$ . Mice gradually increased the number of responses over daily sessions: Main effect of session,  $F[2,10]=8.0$ ,  $p=0.008$ . Increases in response rates were specific to poking on the laser-paired hole: Laser  $\times$  session interaction effect:  $F[2,10]=13.7$ ,  $*p=0.001$ . During laser-off extinction tests, mice poked significantly more on the laser-paired hole, paired t-test  $t[5]=16.3$ ,  $**p<0.001$ . **G.** R-NG→NTS optical stimulation induces place preferences. *Left panel:* Representative heat map showing the pre-test baseline (upper) and on-line place preference (lower). *Right panel:* Place preference for laser-paired side, N=6; paired t-test  $t[5]=7.2$ ,  $*p=0.001$ . **H.** R-NG→NTS optical stimulation induces flavor preferences. Post-conditioning flavor preferences for laser-paired flavors N=6; paired t-test  $t[5]=14.8$ ,  $*p<0.001$ . For one-sample t-tests against 50% (indifference) preferences: Preconditioning:  $t[5]=0.1$ ,  $p=0.89$ ; Post-conditioning,  $t[5]=10.8$  Bonferroni-corrected  $p<0.0001$ . **I.** R-NG→NTS optical stimulation reduces chow intake. N=5, three daily sessions (laser on day 2), one-way RM-ANOVA  $F[2,8]=34.6$ ,  $*p<0.0001$ . **J.** Optical stimulation of R-NG→NTS, but not R-NG→AP, induced robust satiety during 5% IntraLipid intake tests. Shaded blue area indicates sessions when laser was ON. N=5, two-way mixed effects ANOVA, group  $\times$  session interaction:  $F[8,64]=7.8$ ,  $*p<0.001$ . **K.** Optical stimulation of RNG→NTS, but not R-NG→AP, fibers induced robust dopamine release in dorsal striatum. Shaded blue area indicates sessions when laser was ON. N=5, two-way mixed effects ANOVA between-group  $\times$  time interaction effect  $F[15,120]=3.4$ ,  $*p<0.0001$ . **L.** Cre-EBFP and DIO-ChR2-EYFP detected in L-NG. Bar=100 $\mu$ M. **M.** *Left panel:* Vagal nerve fiber activity upon light stimulation of L-NG DIO-ChR2-EYFP-positive neurons. Responses were mostly locked to light pulses (blue bars on top). *Right panel:* Supra-threshold events during nerve recordings. N=12; paired t-test  $t[11]=4.7$   $*p=0.001$ . **N.** L-NG DIO-ChR2-EYFP-positive terminals substantially innervated AP at more caudal (*i*) but not anterior (*ii*) levels (10 $\times$ ). Lower panels show the delimited areas at 40 $\times$ . NTS (**b and d**) innervation was weaker than AP (**a and c**) at more caudal (*i*) but not anterior (*ii*) levels. Bar=100 $\mu$ M. **O.** Optical fibers above L-NG terminals in AP. **P.** LNG→AP optical stimulation failed to sustain self-stimulation. N=5; Two-way RM-ANOVA, Laser  $\times$  session interaction effect:  $F[2,8]=0.7$ ,  $p=0.5$ . During laser-off extinction tests, mice failed to poke more on the laser-paired hole, paired t-test  $t[4]=0.1$ ,  $p=0.8$ . **Q-R.** L-NG→AP optical stimulation failed to induce online place preferences (laser paired to less preferred location,  $t[4]=1.2$ ,  $p=0.3$ , panel **Q**) or aversions (laser paired to more preferred location,  $t[4]=2.0$ ,  $p=0.1$  panel **R**). **S.** L-NG→AP optical stimulation reduces chow intake. N=5, three daily sessions (laser on day 2), one-way RM-ANOVA  $F[2,8]=16.5$ ,  $*p=0.001$ . **T.** Optical stimulation of L-NG→AP, but not L-NG→NTS, induced satiety during 5% IntraLipid intake. Shaded blue area = laser ON. N=5, two-way mixed effects ANOVA, group  $\times$  session interaction:  $F[8,64]=18.6$ ,  $*p<0.001$ . **U.** Optical stimulation of neither L-NG→AP nor L-NG→NTS induced dopamine release in DS. Shaded blue area = laser ON. N=5, two-way mixed effects ANOVA between-group  $\times$  time interaction  $F[15,120]=0.8$ ,  $p=0.6$ . AP= area postrema; DMV=dorsal motor nucleus of vagus; NTS=nucleus of the tractus solitarius. Data reported as mean $\pm$ SEM.

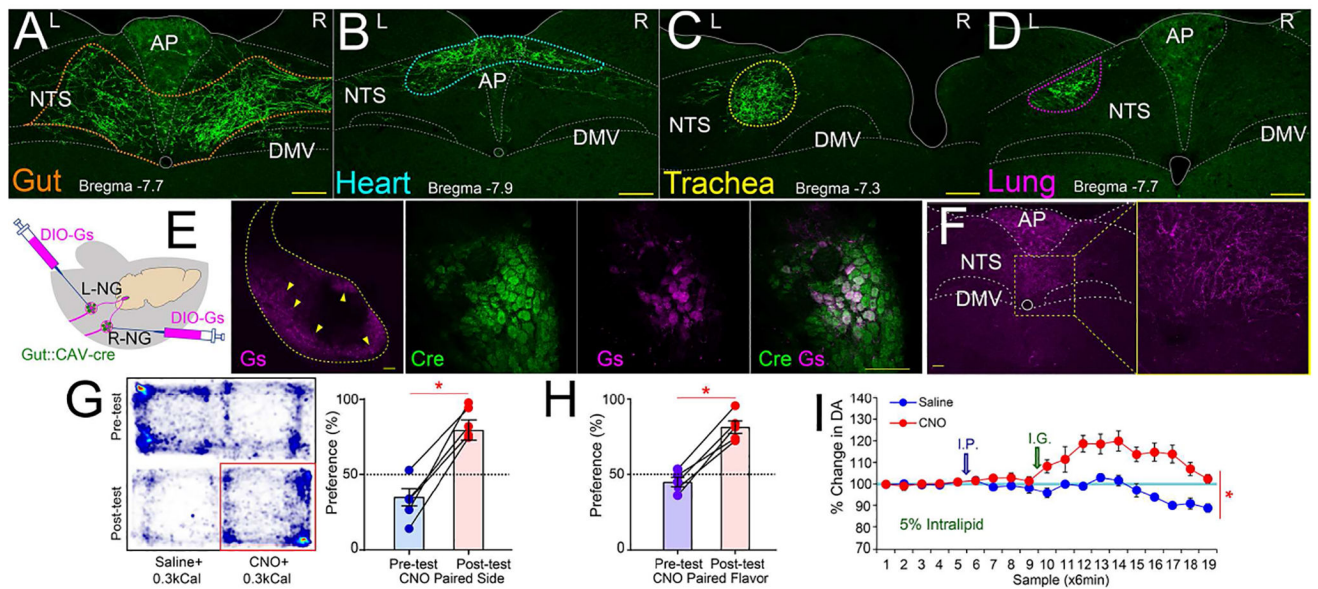


**Figure 2. Organ-specific maps of gut vagal afferents**

**A-D.** The retrograde *Cre*-carrying construct AAVrg-pmSyn1-EBFP-*Cre* was injected into upper gut, heart, lung or trachea. In all cases, DIO-ChR2-EYFP was bilaterally injected into nodose ganglia. Gut (panel **A**), heart (**B**), trachea (**C**), and lung (**D**) terminal sites were restricted to distinctively separate sites within the solitary complex. Additional sections shown in Figures S2A–D. **E.** The upper gut of mice was injected with the retrograde construct CAV2-*Cre*-GFP, and nodose ganglia were bilaterally injected with a *Cre*-inducible AAV-Gs-coupled-mCherry chemogenetic designer receptor construct. CAV2-*Cre*-GFP and AAV-DIO-GsmCherry were detected in nodose ganglia bilaterally. *Middle panel:* mCherry expression is restricted to outermost nodose neurons (10 $\times$ , Bar=100 M). *Right panel:* 40 $\times$ , Bar=100 M. **F.** AAV-DIO-Gs-mCherry-infected terminals by injections into both right nodose (terminal fibers in medial NTS) and left nodose (terminal fibers in AP). **G.** CNO injections induce place preferences. During conditioning, in all sessions animals were administered I.G. with IntraLipid (0.3kcal, 0.6ml). CNO injections were then paired to the less preferred side of the cage. *Left panel:* Representative heat map showing the pre-test baseline (upper) and post-CNO preferences (lower). *Right panel:* Place preference for CNO-paired side, N=5; paired t-test  $t[4]=9.2$ ,  $*p=0.001$ . **H.** Post-conditioning flavor preferences for flavors paired with 5% I.G. IntraLipid (0.3kcal, 0.6ml) + CNO vs. 5% I.G. IntraLipid + saline, N=5; paired t-test  $t[4]=9.5$ ,  $*p=0.001$ . For one-sample t-tests against 50% (indifference) preferences: Pre-conditioning:  $t[4]=1.6$ ,  $p=0.18$ ; Post-conditioning,  $t[4]=7.5$ , Bonferroni-corrected  $p=0.004$ . **I.** CNO injections significantly enhanced dopamine release in dorsal striatum induced by 5% I.G. IntraLipid (0.3kcal, 0.6ml), N=6; Two-way RM-ANOVA CNO  $\times$  sampling time interaction effect  $F[18,72]=7.59$ ,  $*p<0.0001$ . AP= area postrema; DMV=dorsal motor nucleus of vagus; NTS=nucleus of the tractus solitarius. Data reported as mean $\pm$ SEM.

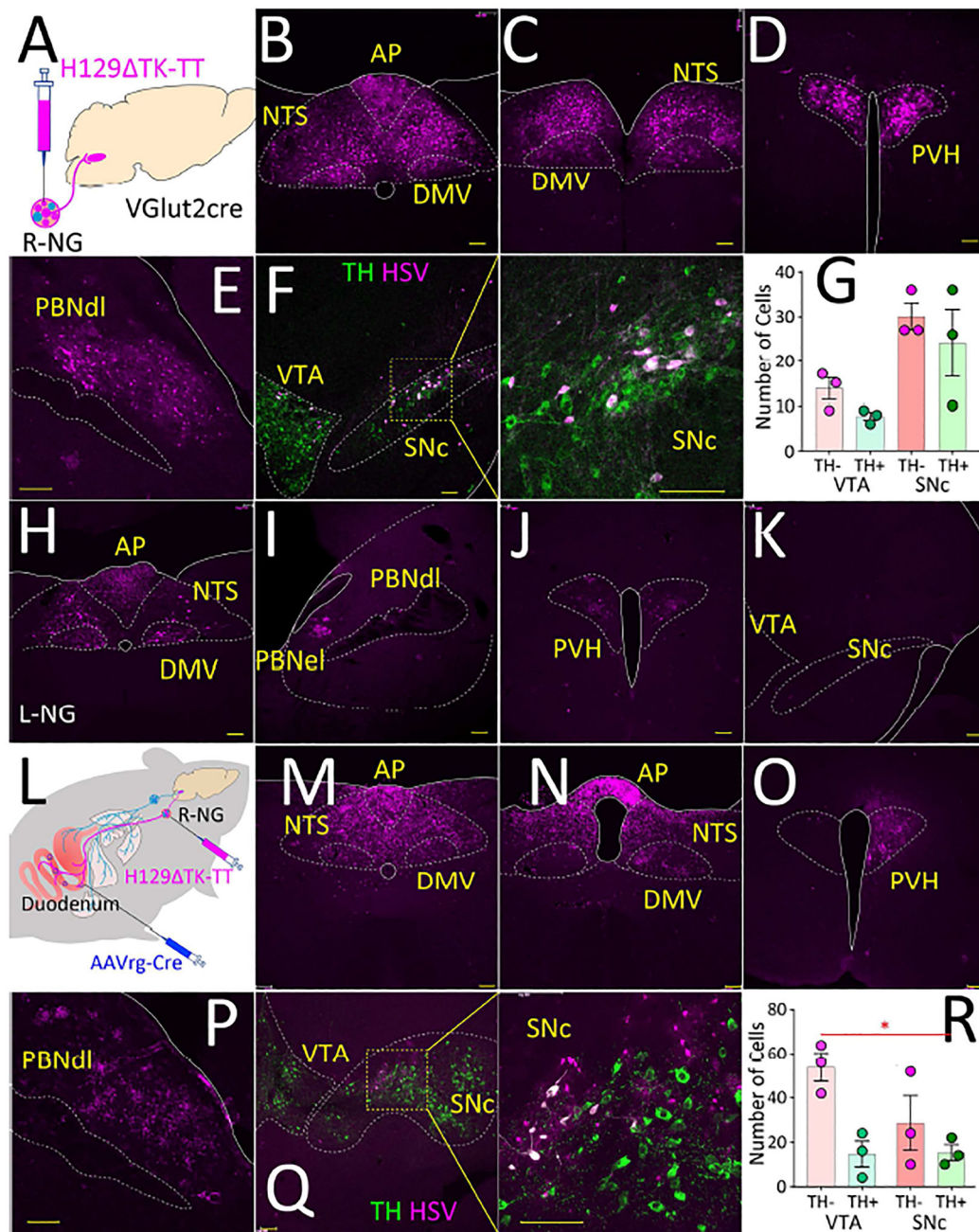


### Figure 3. Transsynaptic labeling of central vagal pathways

**A.** VGlut2-ires-Cre mice were injected with the Cre-inducible, transsynaptic Herpes Simplex Viruses 1 strain H129 TK-TT into the right nodose ganglion (R-NG). **B-C.** Forty-eight hours after the injections, infection was restricted to the dorsal vagal complex (AP, DMV, NTS) at more caudal (**B**) and rostral (**C**) levels. **D-E.** Seventy-two hours after injection infection was detected at NTS targets including PVH and PBNdl. **F.** Ninety-six hours after injections infection was detected in SNc, including in dopaminergic, tyrosine hydroxylase-positive (TH, green) cells. **G.** Numbers of herpes-infected cells in SNc and VTA, including both GABAergic and TH+ cells (values correspond to average numbers of

infected cells per section, N=3 mice). **H-K.** The left nodose ganglion (L-NG) was injected with H129 TK-TT. Infection was observed in the dorsal vagal complex (AP, DMV, NTS), PVH, PBNeI. Note absence of herpes labeling in PBNdl, VTA and SNc. **L.** Upper gut transfected with AAVrg-pmSyn1-EBFP-*Cre*, right nodose ganglion (R-NG) then injected with H129 TK-TT. **M-Q.** Infection was observed in the dorsal vagal complex (AP, DMV, NTS), PVH, PBNdl, PBNeI, and SNc. **R.** Numbers of herpes-infected cells in SNc and VTA, including both GABAergic and TH+ cells (values correspond to average numbers of infected cells per section, N=3 mice, main effect of cell type  $F[1,2]=28.76$ ,  $*p=0.03$ ). *AP* = *area postrema*; *DMV* = dorsal motor nucleus of the vagus; *NTS* = nucleus of the solitary tract; *PBNdl* = parabrachial nucleus, dorsolateral region; *PBNeI* = parabrachial nucleus, externolateral part; *PVH* = paraventricular nucleus of the hypothalamus; *SNc* = *Substantia nigra, pars compacta*; *VTA* = ventral tegmental area. Bars=100 $\mu$ M. Data reported as mean  $\pm$ SEM.

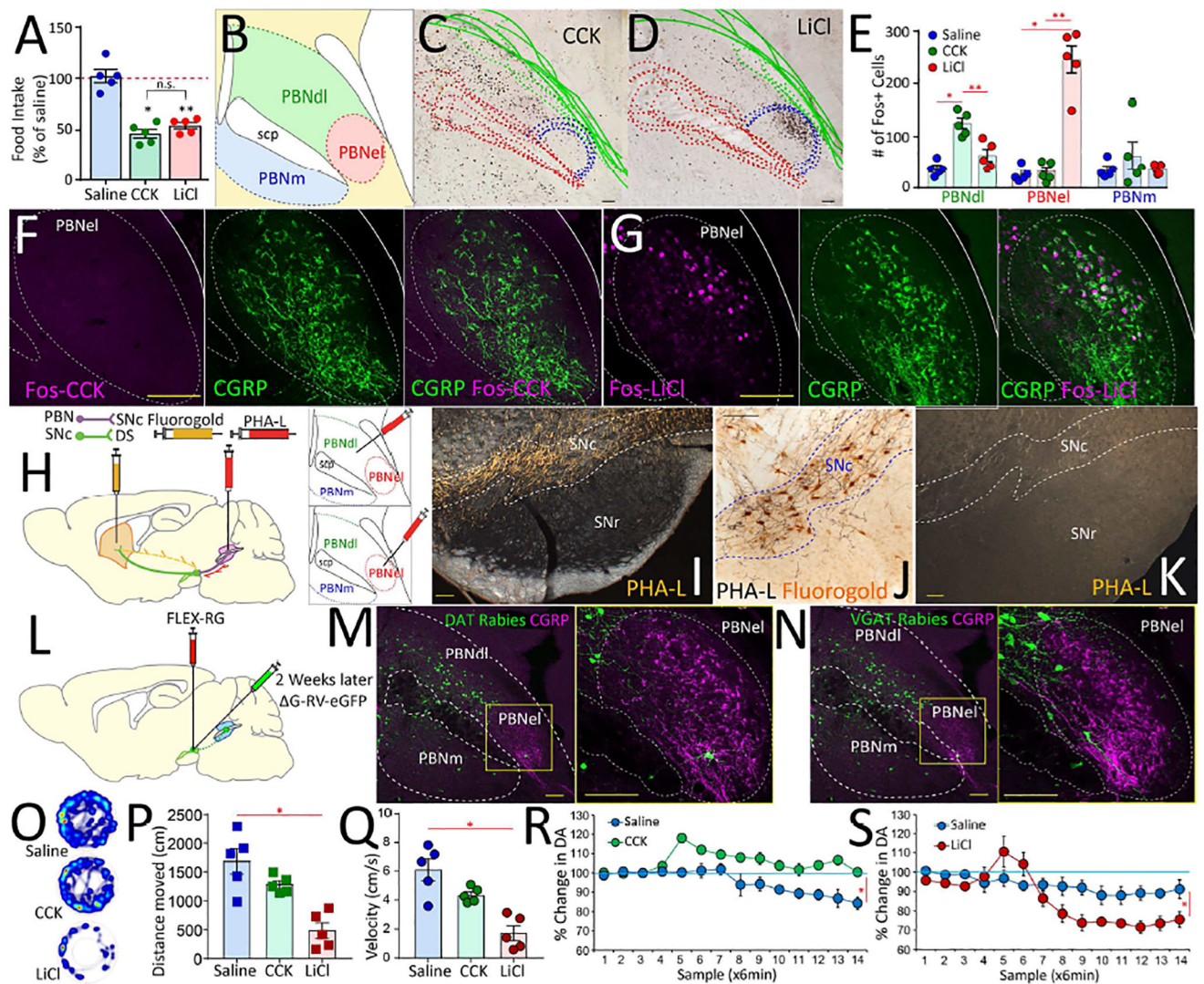


#### Figure 4. Valence-specific organization of the lateral parabrachial area

**A.** Intraperitoneal doses of CCK and LiCl, were titrated to induce ~50% reduction in food intake. Main effect of treatment  $F[2,12]=38.65$   $p<0.001$ .  $N=5$ ; Paired t-test saline vs. CCK Bonferroni  $p<0.001$ ; saline vs. LiCl Bonferroni  $p<0.001$ ; CCK vs. LiCl  $p=0.8$ . **B.** The mouse parabrachial area. *PBNdl* = parabrachial nucleus, dorsolateral region; *PBNel* = externolateral parabrachial nucleus; *PBNm* = medial parabrachial nucleus; *scp* = superior cerebellar peduncle (*brachium conjunctivum*). **C-D.** Compounded image of parabrachial sections showing Fos expression patterns in response to CCK (**C**) and LiCl (**D**) across 5 mice. **E.** Fos + cells in response to CCK or LiCl. PBNdl specifically responded to CCK, whereas PBNel specifically responded to LiCl. No responses for saline injections.  $N=5$  in each group. Main effect of treatment in PBNdl:  $F[2,12]=21.9$ ,  $p<0.0001$ ; Post-hoc two-sample t-tests saline vs. LiCl  $p=0.249$ ; saline vs. CCK Bonferroni  $*p<0.001$ ; LiCl vs. CCK Bonferroni  $**p=0.002$ . Main effect of treatment in PBNel:  $F[2,12]=59.5$ ,  $p<0.0001$ ; Post-hoc two-sample t-tests saline vs. LiCl Bonferroni  $*p<0.001$ ; saline vs. CCK  $p=0.9$ ; LiCl vs. CCK Bonferroni  $**p<0.001$ . Main effect of treatment in medial PBN (PBNm):  $F[2,12]=0.8$ ,  $p=0.471$ ; Post-

hoc two-sample t-tests all  $p > 0.85$ . **F.** No Fos expression in response to CCK was observed in PBNel (left), in particular no CGRP+ neurons (center) were found to express Fos in response to CCK (right). **G.** Robust Fos expression in response to LiCl was observed in PBNel (left). The region containing CGRP+ neurons (center) was found to include most of the LiCl-responding Fos-positive neurons (right). **H.** The anterograde tracer PHA-L was iontophoretically injected into either PBNdl or PBNel; in the same PBNdl case the retrograde tracer FluoroGold was iontophoretically injected into the dorsal striatum. **I.** Darkfield photomicrographs of coronal sections revealing a substantial anterograde labeling in the SNc after an injection in PBNdl. Note that these projection patterns were highly specific, with the *Substantia nigra, pars reticulata* (SNr) devoid of parabrachial terminals. Scale bar 100 $\mu$ m. **J.** Brightfield photomicrograph showing PHA-L anterograde labeling from PBNdl in register with FluoroGold retrograde labeling from the dorsal striatum in the SNc, suggesting the existence of a parabrachio-nigro-striatal pathway. Scale bar 20 $\mu$ m. **K.** Fibers of passage running dorsal to the SNc, itself unlabeled, after an injection in the PBNel. Scale bar 100 $\mu$ m. **L.** To assess the cell-type specificity of the SNc targets of parabrachial projections, we transfected the SNc of both DAT-ires-*Cre* and VGat-ires-*Cre* mice with the construct AAV5-EF1a-FLEX-TVAmCherry, and two weeks later with the *Cre*-inducible retrogradely transported pseudotyped rabies virus SAD G-GFP. **M-N.** In both DAT-ires-*Cre* (**M**) and VGat-ires-*Cre* (**N**) mice, robust expression of rabies-infected cells were observed in PBNdl and to a lesser extent in PBNm on 7 days post rabies infection, but virtually no rabies-infected cells were observed in PBNel, including regions containing CGRP+ cells. Bars=100 $\mu$ m. **O.** Open-field heatmaps after intraperitoneal injections of saline (upper), CCK (center), or LiCl (lower). **P-Q.** LiCl injections significantly reduced distance traveled (**P**) and velocities (**Q**) compared to both saline and CCK. CCK produced no significant effects on either. ANOVA  $F[2,12]=15.9$ ,  $p=0.001$  (distance),  $F[2,12]=16.5$ ,  $p<0.001$  (velocity). Post-hoc t-tests Bonferroni  $*p<0.05$ . **R.** CCK injections significantly enhanced dopamine release in dorsal striatum  $N=5$ ; Two-way RM-ANOVA injection  $\times$  sampling time interaction effect  $F[13,52]=5.8$ ,  $*p<0.0001$ . **S.** LiCl injections significantly inhibited dopamine levels in dorsal striatum  $N=5$ ;  $F[13,52]=29.7$   $*p<0.0001$ . Data reported as mean $\pm$ SEM.

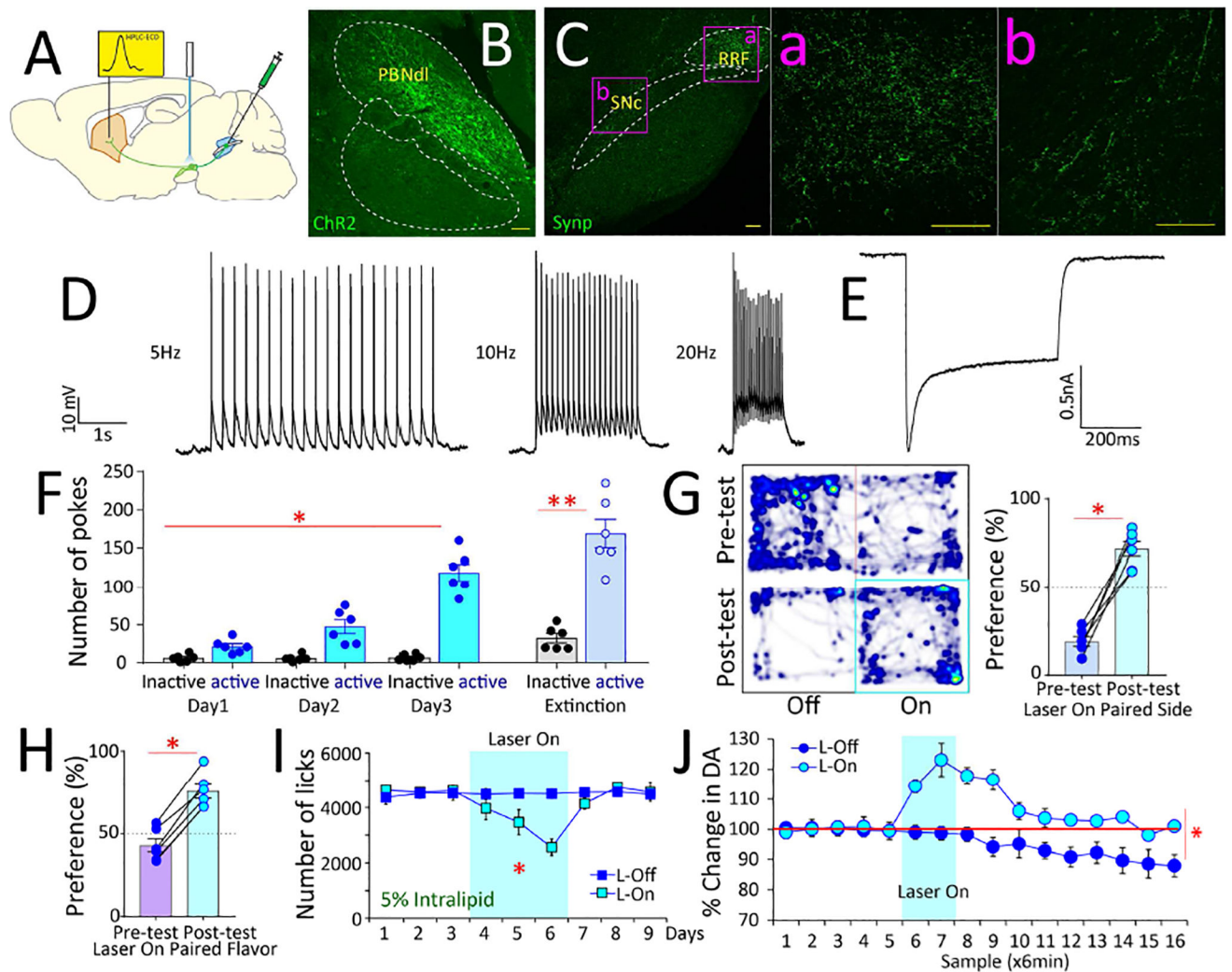


**Figure 5. Optical activation of parabrachio-nigral vs. parabrachio-amygdalar pathways mediate reward vs. avoidance behaviors**

**A.** DIO-ChR2-EYFP was injected into PBNdl of VGlut2-ires-*Cre* mice, and optical fibers placed above parabrachial terminals on SNc (PBNdl[VGlut2]→SNc pathway). Microdialysis cannulae were implanted into the dorsal striatum. **B.** Injection of the DIO-ChR2-EYFP construct was restricted to PBNdl. **C.** Similar injections of *Cre*-inducible synaptophysin-EYFP into the PBNdl of VGlut2-ires-*Cre* mice reveal dense glutamatergic parabrachial terminals in SNc and RRF (magnification shown on panels *Ca*, *Cb*). **D.** Action potentials (current clamp) from ChR2-expressing VGlut2 neurons in PBNdl upon optogenetic stimulation. **E.** Inward membrane current recorded in VGlut2-ChR2 neurons under voltage clamp. Blue bar, the application of the LED-generated blue light pulse. **F.** PBNdl[VGlut2]→SNc optical stimulation sustains self-stimulation behavior. N=6; Two-way RM-ANOVA, Main effect of poking on the laser-paired hole vs. inactive hole  $F[1,5]=88.0$ ,  $p<0.001$ . Mice gradually increased the number of responses over daily sessions: Main effect of session,  $F[2,10]=62.8$ ,  $p<0.001$ . Increases in response rates were specific to poking on the laser-paired hole: Laser × session interaction effect:  $F[2,10]=69.5$ ,  $*p<0.001$ . During laser-

off extinction tests, mice poked significantly more on the laser-paired hole, paired t-test  $t[5]=6.589$ ,  $**p=0.001$ . **G.** PBNdl[VGlut2]→SNc optical stimulation induces place preferences. The laser source was switched ON whenever the mouse was detected on the less preferred side of the cage. *Left panel:* Representative heat map showing the pre-test baseline (upper) and on-line place preference (lower). *Right panel:* Place preference for laser-paired side,  $N=6$ ; paired t-test  $t[5]=9.5$ ,  $*p=0.001$ . **H.** PBNdl[VGlut2]→SNc optical stimulation induces flavor preferences. Post-conditioning flavor preferences for laser-paired flavors  $N=6$ ; paired t-test  $t[5]=14.6$ ,  $*p<0.001$ . For one-sample t-tests against 50% (indifference) preferences: Pre-conditioning:  $t[5]=1.8$ ,  $p=0.127$ ; Post-conditioning,  $t[5]=5.9$ , Bonferroni-corrected  $p=0.002$ . **I.** PBNdl[VGlut2]→SNc optical stimulation during ingestion of 5% IntraLipid. After daily baseline sessions 1–3, intake is reduced during laser ON sessions 4–6, and immediately returned to baseline on post-laser sessions 7–9.  $N=6$ , two-way RM-ANOVA laser × session interaction effect  $F[8,40]=9.4$ ,  $*p<0.001$ . **J.** PBNdl[VGlut2]→SNc optical stimulation induces significant dopamine release in dorsal striatum,  $N=6$ , two-way RM-ANOVA laser × sampling time interaction effect  $F[15,60]=7.1$ ,  $*p<0.0001$ . *PBNdl* = parabrachial nucleus, dorsolateral part; *SNc*: *Substantia nigra, pars compacta*; *RRF* = retrorubral field. Bars=100 $\mu$ M. Data reported as mean $\pm$ SEM.

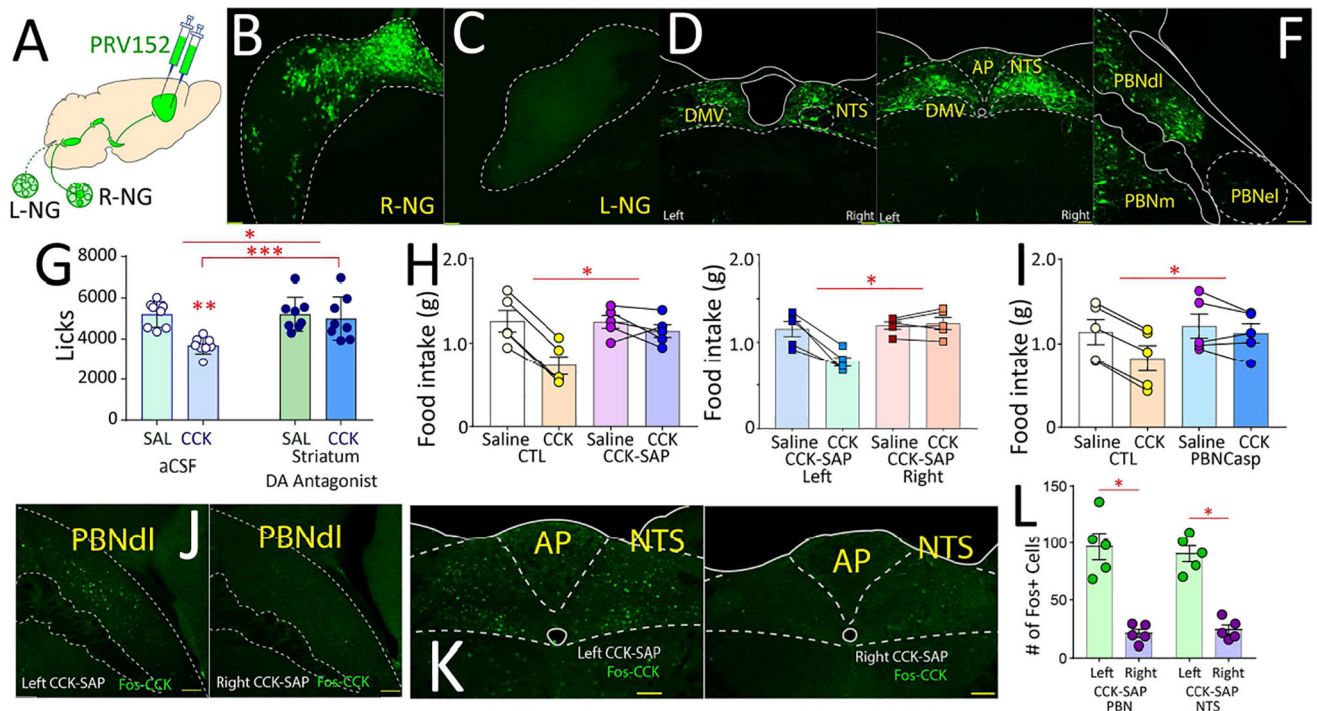


**Figure 6. Right nodose-parabrachio-nigral pathway is required for vagal effects on food intake**  
**A-F.** The polysynaptic pseudorabies PRV152-GFP was injected bilaterally into dorsal striatum. Dense retrograde labeling was observed in right (**B**), but not left (**C**), nodose ganglion. In NTS, labeling observed in medial rostral (**D**) and caudal (**E**) areas restricted to gut terminal fields. In PBN (**F**), labeling restricted to dorsolateral gut terminal fields. **G.** Dopamine receptor antagonism DS abolished satiating effects of CCK; N=8, two-way RM-ANOVA main effects of antagonist F[1,7]=5.124,  $p=0.058$ ; CCK F[1,7]=47.7,  $p<0.001$ ; antagonist  $\times$  CCK F[1,7]=13.3,  $p=0.006$ . Post-hoc t-tests: CCK + striatal aCSF vs. saline + striatal aCSF Bonferroni  $*p<0.001$ ; CCK + striatal aCSF vs. CCK + striatal antagonist Bonferroni  $p>0.08$ . **H. Left panel:** Right, but not left, gut vagal deafferentation abolished satiating effects of CCK (group F[1,8]=8.7,  $*p<0.02$ ; injection  $\times$  group F[1,8]=19.6,  $*p=0.002$ ). **Right panel:** Bilateral deafferentation produces similar effects to right deafferentation (two-way mixed ANOVA injection  $\times$  group F[1,8]=18.4,  $*p=0.003$ ). **I.** PBNdl $\rightarrow$ Snc lesions abolished the suppressive effects of CCK on food intake: N=5 in each group, main effects of CCK F[1,8]=33.1,  $p<0.001$ ; lesion F[1,8]=0.89,  $p=0.37$ ; CCK  $\times$  lesion F[1,8]=11.0,  $*p=0.01$ . **J-L.** Right, but not left, gut vagal deafferentation abolished Fos expression induced by CCK in PBNdl (**J**, left, left deafferentation, right, right deafferentation) and NTS (**K**, left, left deafferentation, right, right deafferentation). Panel **L** quantifies Fos+ cells. N=5, One sample t-test, PBN:  $t[8]=6.183$ , Bonferroni  $*p<0.001$ ; NTS:  $t[8]=8.202$ , Bonferroni  $*p<0.001$ . AP = area postrema; DMV = dorsal motor nucleus of the vagus; NTS = nucleus of the solitary tract; PBNdl = parabrachial nucleus, dorsolateral region; PBNel = parabrachial nucleus, externolateral part; PBNm = medial parabrachial nucleus. Data reported as mean $\pm$ SEM.